

We are IntechOpen, the world's leading publisher of Open Access books Built by scientists, for scientists

6,900

Open access books available

186,000

International authors and editors

200M

Downloads

Our authors are among the

154

Countries delivered to

TOP 1%

most cited scientists

12.2%

Contributors from top 500 universities



WEB OF SCIENCE™

Selection of our books indexed in the Book Citation Index
in Web of Science™ Core Collection (BKCI)

Interested in publishing with us?
Contact book.department@intechopen.com

Numbers displayed above are based on latest data collected.
For more information visit www.intechopen.com



Effects of Electron Irradiation Upon Absorptive and Fluorescent Properties of Some Doped Optical Fibers

Alexander V. Kir'yanov

Additional information is available at the end of the chapter

<http://dx.doi.org/10.5772/63939>

Abstract

A review of the recent studies of the effect of irradiating silica-based fibers doped with rare earths and metals by a beam of high-energy (β) electrons is presented. Of the review's main scope are the attenuation spectra' transformations occurring in optical fiber of such types under electron irradiation, allowing, from one side, to recover some general essence of the phenomena involved and, from the other side, to draw the features that would make such fibers useful for applications, for example, in dosimetry and space technologies. Among the fibers of the current review's choice, exemplifying the effect of electron irradiation most brightly, are ytterbium (Yb) and cerium (Ce) (the rare earths' representatives) and bismuth (Bi) (the post-transitional metals representative) doped fibers, where a diversity of the electron-irradiation-related effects is encouraged.

Keywords: electron irradiation, ytterbium-, cerium- and bismuth-doped silica fibers, photodarkening, optical bleaching

1. Introduction

In this chapter, a few examples are demonstrated of the impact of high-energy (β) electrons irradiation on the absorptive and fluorescence properties of silica-based optical fibers doped with rare earths and metals. The results presented hereafter seem to be useful for understanding the processes standing behind the highlighted phenomena and for possible applications of the fibers, say, in dosimetry and space technology.

In each case, we used for irradiating fiber samples a controllable linear accelerator of the LU type that emits β -electrons with a narrow-band energy spectrum (~ 6 MeV) in a short-pulse (~ 5 μ s) mode. The samples with lengths of around 1–2 m were placed into the

accelerator's chamber for various time intervals, which provided growing irradiation doses. The irradiated fibers were then left for 2 weeks prior to the main-course spectral measurements to avoid the role of short-living components in the decay of induced absorption (IA). The measurements were done during a limited time (viz., the following 2...3 weeks) for diminishing the effect of spontaneous IA recovering. Note that ionization, that is, the production of β -induced carriers by an electron beam (i.e., of secondary free holes and electrons), is the main cause of the spectral transformations in the fibers. This happens because high-energy primary β -electrons are virtually nondissipating at the propagation through a fiber sample; on the other hand, certain contribution in ionization of the fibers' core-glasses arising from γ -quanta born at inelastic scattering of the high-energy electrons cannot be disregarded.

We demonstrate below first a study of the resistance of a couple of cerium (Ce)-doped alumino-phospho-silicate fibers (one of them being codoped with gold (Au)), to β -electrons. The experimental data reveal a severe effect of β -irradiation upon the fibers' absorptive properties, given by noticeable susceptibility of Ce ions being in $\text{Ce}^{3+}/\text{Ce}^{4+}$ states to the treatment, arising as growth followed by saturation of IA. We also report the essentials of posterior bleaching of β -darkened fibers, also in terms of attenuation spectra' transformations, at exposing them to low-power green (a He-Ne laser) and ultra violet (UV, a mercury lamp) light. It is shown that both phenomena are less expressed in Ce fiber codoped with Au than in Au-free one and that the spectral changes in the former are more regular versus dose and bleaching time.

Then, we provide a comparative experimental analysis of IA, induced by β -electrons, for a series of ytterbium (Yb)-doped alumino-germano-silicate fibers with different concentrations of Yb^{3+} ions and compare this effect with the photodarkening (PD) phenomenon in the same fibers, arising at resonant (into 977 nm absorption peak of Yb^{3+} ions) optical pumping. The experimental data obtained reveals that, in these two circumstances, substantial and complex but different in appearance changes affecting the resonant absorption band of Yb^{3+} ions and the off-resonance background loss are produced in the fibers.

Finally, we report a study of attenuation spectra' transformations in a set of bismuth (Bi)-doped silica fibers with various contents of emission-active Bi centers, which occur as the result of β -irradiation. Among the data obtained, notice a substantial decrease of concentration of Bi centers, associated with the presence of Germanium (Ge) in core-glass, with increasing irradiation dose (the "bleaching" effect), while, on the contrary, an opposite trend, that is, dose-dependent growth of resonant-absorption ascribed to Bi active centers, associated with the presence in core-glass of Aluminium (Al). These results are worth noticing for understanding the nature of Bi-related centers in silica fibers, yet uncovered.

2. The effects of electron irradiation and posterior optical bleaching in Ce-doped and Ce/Au-codoped alumino-phospho-silicate fibers

Development of suitable host glasses and fibers for dosimetry, which are based on formation of radiation-induced defects leading to glass coloration [1–6] or filling pre-existing traps,

measured by means of thermally or optically stimulated fluorescence [7], became a hot task. Dosimetry systems can be used in high radiation fields, for example, in proximity to nuclear reactors, hazardous places, and in open space. Fiber-based dosimeters are being intensively investigated and recently a few systems have been proposed, based on versatile physical effects in radiation-sensitive silica fibers [8].

Cerium (Ce)-doped silica glass has interesting fluorescent properties [9], which makes it promising for utilizing as a scintillator for detecting X- and γ -rays, or neutrons [10, 11]. On the other hand, silica glass is known to suffer from the presence of point defects and OH groups, responsible for nonradiative recombination channels competing fluorescence. In turn, Au, when combined with cerium oxide (CeO_2) is known to be a promising catalyst for the reaction $\text{CO} + \text{H}_2\text{O} \rightarrow \text{H}_2 + \text{CO}_2$ [12, 13], giving a way to remove carbon-related impurities along with OH groups from silica matrix during synthesis. Thus, Ce/Au codoped glass is expected to enhance efficiency of energy transfer from the host matrix to emissive centers. The other motivation for Au codoping is to increase radiation resistance of Ce-doped fiber, as argued in more details below. The refereed properties of alumino-phospho-silicate glass doped with Ce and Ce/Au are also a concern of optical fibers made on its base.

Below, the results of experiments on irradiating Ce-doped alumino-phospho-silicate fibers by energetic β -electrons are highlighted, resulting in the fibers darkening. It is furthermore shown that the irradiated fibers are sensitive to weak light of a He-Ne laser (543 nm) and UV mercury lamp, both leading to partial recovery of their initial properties. The whole of experimental data evidences notable susceptibility of Ce-doped fibers to both kinds of treatment. As well, it is demonstrated that the spectral transformations occurring in Ce fiber codoped with Au are less expressed but more regular upon β -irradiation dose and exposure time when bleaching than those in Au-free fiber. A brief discussion in attempt of a reasonable explanation of the experimental laws completes the study, with the key point being a discussion about the species involved in the processes, which are associated with Ce.

The reported results may have value for using Ce-doped silica fibers for dosimetry in harmful environments [8, 14–20] and inscribing Bragg gratings [21–25]. As well, these results seem to be impactful, given by renewed interest to Ce codoping as a tool for diminishing PD in Yb-doped fibers (we inspect the last effect in detail in Paragraph 3).

2.1. Fiber samples and experimental arrangement

The sourcing Ce-doped and Ce/Au-codoped fiber preforms based on alumino-phospho-silicate glass have been made by means of modified chemical vapor deposition (MCVD) process employed in conjunction with solution doping (SD) technique; the final fibers have been drawn from the preforms using a drawing tower. Core diameters/numerical apertures of the two fibers were measured to be $\sim 25 \mu\text{m}/0.15\dots 0.16$, respectively.

Estimated from EDX, average doping levels were found to be 5.0 wt.% Al_2O_3 , 0.15 wt.% P_2O_5 , 0.3 wt.% CeO_2 (in the Ce-doped fiber) and 5.1 wt.% Al_2O_3 , 0.15 wt.% P_2O_5 , 0.27 wt.% CeO_2 , and 0.2 wt.% Au_2O_3 (in the Ce/Au-codoped fiber). Both fibers had multimode wave-guiding, which make them useful for sensor applications. A sample of standard multimode Al-doped (~ 6 wt.

% Al_2O_3) fiber was used in experiments for comparison. The β -irradiation dosage below corresponds to 1×10^{12} ("dose 1"), 5×10^{12} ("dose 2"), 1×10^{13} ("dose 3"), 5×10^{13} ("dose 4"), 1×10^{14} ("dose 5"), and 2.5×10^{15} ("dose 6") cm^{-2} .

Optical transmission spectra of fiber samples were measured (employing the cutback method), using a white light source and optical spectrum analyzer (OSA), turned to a 5 nm resolution. Such spectra were recorded before and after each stage of β -irradiation and at posterior exposure to light of a He-Ne laser (543 nm) or UV lamp ($\lambda < 450$ nm). The attenuation spectra presented below were obtained after recalculating the measured transmissions into loss [dB/m]. In some of the figures below the difference spectra in terms of IA are provided, which were obtained after subtraction of the attenuation spectra of pristine samples from the ones taken after a certain dose of β -irradiation; this allows one straightforward view on the "net" spectral loss changes in the darkened fibers. The transmission dynamics at optical bleaching of β -darkened fibers by 543 nm light was inspected applying "frontal" detecting geometry where a beam of the He-Ne laser was coupled into a fiber sample, while the transmitted light was detected using a Si photodetector; this permitted detection of the changes in transmission *in situ*. The results of the measurements are given below in terms of absorption difference (AD) at bleaching with respect to the initial (β -darkened) state of the fiber. The experiments on optical bleaching of β -irradiated fibers by UV light were as well proceeding *in situ*, where transmission change at long-term exposure to UV light was analyzed. All experiments were made at room temperature.

2.2. Experimental

2.2.1. IA as a result of β -irradiation

In **Figure 1**, we demonstrate (a) attenuation spectra of the Ce-doped (black solid curve 1) and Ce/Au-codoped (grey dashed curve 2) fibers before irradiation, that is, in their "pristine" state, and (b and c) the fibers' cross-sections, obtained at white light illumination. Long (meters)

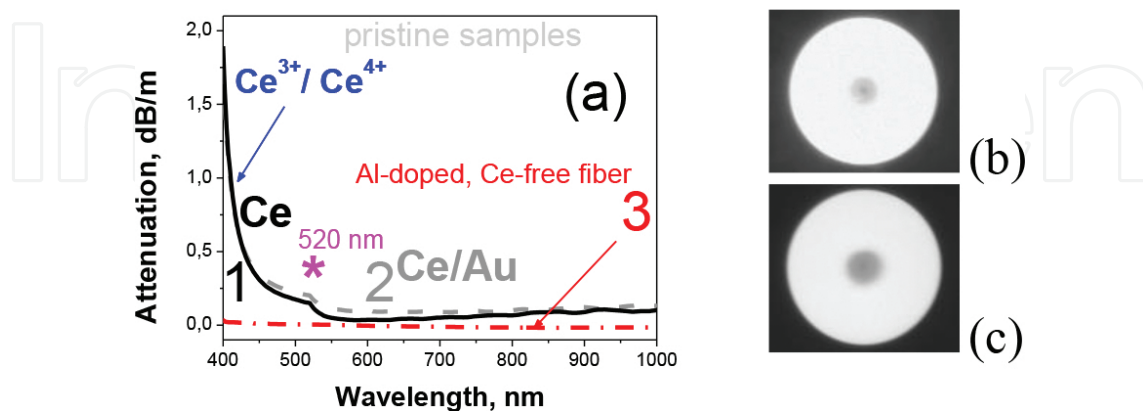


Figure 1. (a) Attenuation spectra of pristine Ce-doped (1), Ce/Au-codoped (2), and Al-doped Ce-free (3) fibers in a VIS-to-near-IR spectral range and micro-photographs of pristine Ce-doped (b) and Ce/Au-codoped (c) fibers. (Reproduced with permission from Kir'yanov et al. [75]. Copyright© 2014, Optical Society of America).

fibers were used in the measurements applying the cutback method, whereas short (10 centimeters) pieces of fibers—at microscopy. For comparison, spectral loss of “standard” Al-doped Ce-free fiber is presented in **Figure 1(a)**—see red dash-dotted curve 3.

We reveal from (a) that, in both Ce-doped and Ce/Au-codoped fibers, dramatic growth of absorption occurs toward UV, below ~550 nm, which is known to be a shoulder of the strong absorption bands adherent to Ce³⁺/Ce⁴⁺ ions (mostly located in UV [23, 24]), and that no such feature is observed in the reference Ce-free fiber. Also notice steep loss rise in Ce-doped and Ce/Au-codoped fibers toward IR and a small peak at ~520 nm (asterisked), the features not observed in case of the Ce-free fiber.

Figure 2 shows the trends occurring in the fibers’ attenuation spectra as the result of β -irradiation at moderate dose 4. Note that in this case, the measurements were proceeding with shorter fiber samples (~a few cm) in virtue of strong IA, established after β -irradiation.

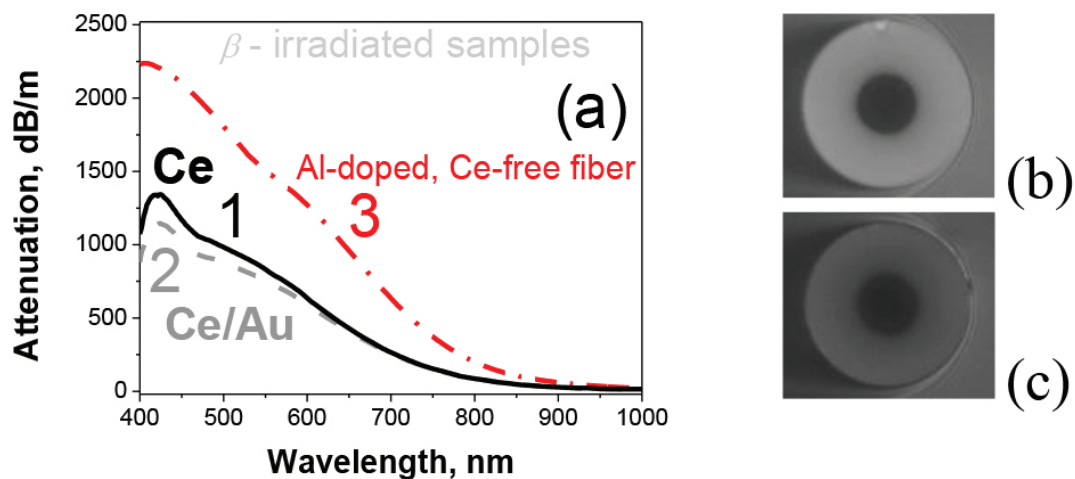


Figure 2. (a) Attenuation spectra of Ce-doped (1), Ce/Au-codoped (2), and Al-doped cerium-free (3) fibers, all measured after β -irradiation with dose 4 ($5 \times 10^{13} \text{ cm}^{-2}$) and micro-photographs of Ce-doped (b) and Ce/Au-codoped (c) fibers recorded after irradiation with this dose. (Reproduced with permission from Kir’yanov et al. [75], Copyright© 2014, Optical Society of America).

It is seen that IA in the Ce-free fiber is ~two times bigger than in the Ce-doped and Ce/Au-codoped ones. The other fact is that IA maxima are located near 400 and 500 nm in these two fibers, whereas the ones in the Ce-free one—at ~400 and ~600 nm, that is, in the range most probably attributing to well-known nonbridging oxygen-holes (NBOHCs) [26] (while the presence of other defect states in it—such as Si-/Al-defect centers cannot be excluded). Furthermore, it is seen from photos (b) and (c) that, in the Ce-doped and Ce/Au-codoped fibers, the core and adjacent core-cladding areas suffer darkening after β -irradiation, in the former, the effect being more pronounced.

Figure 3 demonstrates that IA in the Ce-doped (a) and Ce/Au-codoped (b) fibers increases monotonously with dose; this trend is noticeable for the 400–700 nm range, while for bigger wavelengths it fades. The other detail seen is that for moderate doses (1–4), IA is stronger in the Ce-doped fiber.

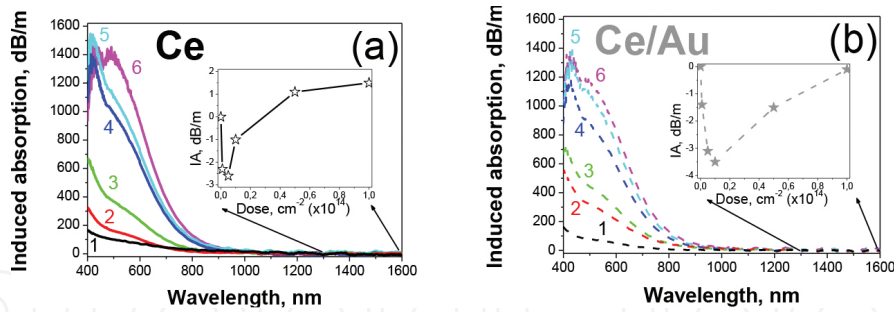


Figure 3. Main frames: IA spectra of Ce-doped (a) and Ce/Au-codoped (b) fibers; curves 1–6 correspond to doses of irradiation (in both figures) being: 1×10^{12} (1), 5×10^{12} (2), 1×10^{13} (3), 5×10^{13} (4), 1×10^{14} (5), and 2.5×10^{15} (6) cm^{-2} . Insets: average IA-losses measured within the 1300–1550 nm range *vs.* irradiation dose. (Reproduced with permission from Kir'yanov et al. [75]. Copyright© 2014, Optical Society of America).

The two-peaks structure of the IA spectra is apparent at higher irradiation doses for both fibers, with the first peak (bigger in magnitude) locating at $\sim 415 \pm 10$ nm and the second one (lower in magnitude)—at $\sim 520 \pm 10$ nm (compared to the ~ 520 nm peak asterisked in the attenuation spectra of pristine fibers in **Figure 1(a)**). To evaluate IA strength in the fibers in function of β -irradiation dose, let us compare the IA spectra with the attenuation spectra of the same fibers being in pristine state (refer to **Figure 1**). It is known that attenuation growth toward UV is common for Ce-doped glass, as stemming from the transitions inherent to $\text{Ce}^{3+}/\text{Ce}^{4+}$ ions. (Unfortunately, IA arising in the UV-region, below 400 nm, was undetectable using our experimental equipment.) Regarding IA in the near-IR, note that the spectral transformations in this region are more complex (see insets to **Figure 3**) whose nature is unclear at the moment.

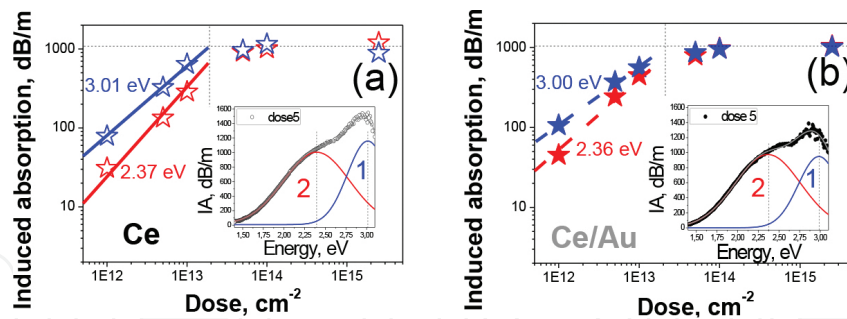


Figure 4. Main frames: dose dependences of IA for Ce-doped (a) and Ce/Au-codoped (b) fibers; blue and red symbols and lines show IA magnitudes of bands 1 and 2, obtained after deconvolution of the spectra shown in **Figure 3**. Insets: examples of deconvolution of the data obtained for the fibers, irradiated with dose 5 (spectra are plotted in eV-domain). (Reproduced with permission from Kir'yanov et al. [75]. Copyright© 2014, Optical Society of America).

Deconvolution of IA spectra (**Figure 3**) allows a closer view on their two-band structure (see insets in **Figure 4(a) and (b)**). Spectral locations of the bands (1 and 2) were found to be almost independent of irradiation dose, for both fibers: they are centered at ~ 3.0 and $\sim 2.4 (\pm 0.1)$ eV and are measured in half-widths at a 3 dB level by ~ 0.3 and $\sim 0.5 (\pm 0.05)$ eV, respectively. In main frames of **Figure 4**, IA—in terms of these two peaks' magnitudes—is plotted versus irradiation dose; these dependences are shown, respectively, by blue (band 1) and red (band

2) symbols. Fitting them within domain of smaller doses (up to $\sim 2 \times 10^{13} \text{ cm}^{-2}$), linear growth of IA in both bands versus dose is revealed (see the blue and red lines in the figure).

The slopes' values estimated as the result of fitting were found to be ~ 1.7 ($\sim 1.2 \text{ dB/m/cm}^2$) (Ce-doped fiber) and ~ 1.3 ($\sim 0.9 \text{ dB/m/cm}^2$) (Ce/Au-codoped fiber), correspondingly, for bands 2 and 1. It deserves mentioning that these ratios, on one hand, are almost equal for both fibers (~ 1.5) and, on the other hand, the slopes' ratios, when compared for bands 1 and 2, are vastly equal as well (~ 1.3). Furthermore, at bigger irradiation doses IA, in both bands and for either fiber, steadily approaches the "plateaus", marked by black dotted lines in the figures. It is interesting that IA in maxima of bands 1 and 2 at the plateaus (i.e. at doses exceeding $2 \times 10^{14} \text{ cm}^{-2}$) has virtually the same magnitude, for both fibers.

2.2.2. Bleaching of IA as a result of posterior exposure to 543 nm/UV light

Hereafter, the featuring data on optical bleaching of β -irradiated Ce-doped and Ce/Au-codoped fibers by a low-power He-Ne 543 nm laser and UV mercury lamp are reported.

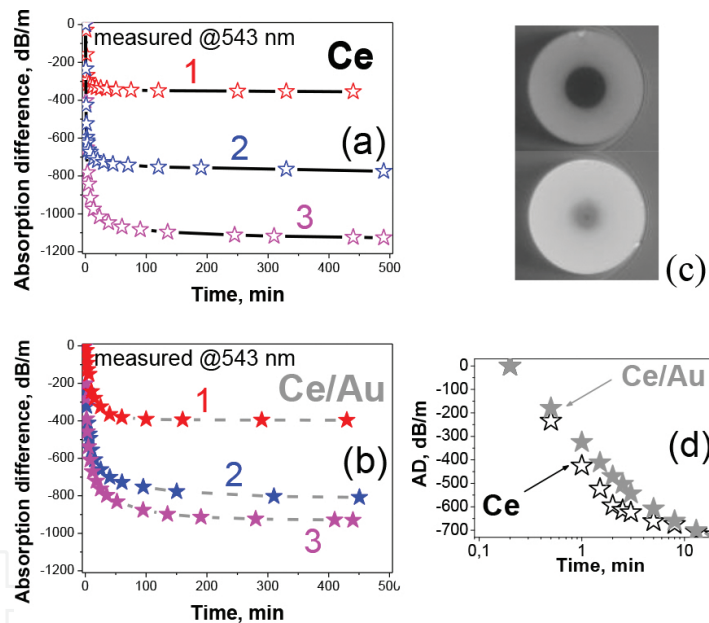


Figure 5. Dynamics of attenuation decay in terms of AD in Ce-doped (a) and Ce/Au-codoped (b) fibers under the action of 543 nm light ($\sim 0.5 \text{ mW}$); bleaching (negative AD) was realized after β -irradiation with doses 2 (curves 1), 4 (curves 2), and 6 (curves 3), for which AD is taken to be zero. (c) Micro-photographs of darkened (dose 5 of β -irradiation) Ce-doped fiber prior to (top) and after bleaching during 7.5 h (bottom). (d) Examples of the initial 543 nm bleaching stage, zooming the dependences shown by curves 2 in (a) and (b), respectively. (Reproduced with permission from Kir'yanov et al. [75]. Copyright© 2014, Optical Society of America).

Keeping in mind that, IA, a signature of color centers or defects in glass matrix produced at different kinds of irradiation, can be "bleached" by light (see e.g. [59–61]), we found reasonable to check whether such treatment has effect in our case.

First, we inspected the effect of weak 543 nm light delivered from a 1.5 mW He-Ne laser. In the experiments, power launched into both fibers was fixed ($\sim 0.5 \text{ mW}$; coupling efficiency

~30%). In this case, very short pieces (1...2 cm) of β -irradiated fibers were handled, given big IA, measured by hundreds of dB/m (refer to **Figures 3 and 4**), being established at β -darkening. The results are shown in **Figure 5**.

In the left part of **Figure 5**, we show the temporal dynamics of changes in attenuation of the Ce-doped (a) and Ce/Au-codoped (b) fibers under the action of 543 nm light, measured at the same wavelength. The effect of partial bleaching of β -induced loss (the negative AD) is apparent. Note that optical bleaching of both fibers demonstrates a saturating behavior and that the decay rate is bigger for the fiber codoped with Au than for Au-free one (compare curves 1–3 in (a) and (b)); also notice an almost exponential character of bleaching when the process gets starting (see (d) on the right side of **Figure 5**). The bleaching effect is clearly demonstrated by the photographs in **Figure 5(c)**, exemplifying the case of Ce-doped fiber. It is seen that its initial state (before β -irradiation) was almost restored under the action of 543 nm light: compare the photos in **Figure 1(b)** and **Figure 5(c)**.

One would speculate on whether bleaching of the Ce-doped and Ce/Au-codoped fibers arises solely due to laser-light-induced recombination or due to thermally assisted recombination, too, but as for us, the former appears to play a vital role.

Figure 6(a) and (b) shows how the bleached (main frames) and unbleached (insets) loss in the Ce-doped and Ce/Au-codoped fibers behave at 543 nm bleaching. Note that unbleached (remnant) loss is bigger in Ce/Au- than in Ce-doped fiber, that is, codoping of a Ce-doped fiber with Au results in a similar property of lesser susceptibility to exterior influence (compare with the results on β -irradiation); however, in the case of bleaching this feature appears to be a disadvantage.

The results of illuminating darkened Ce-doped and Ce/Au-codoped fibers with UV light are shown in **Figure 7**. In **Figure 7(a)** we exemplify the spectral dynamics of transmission of β -irradiated (at dose 5) Ce/Au-codoped fiber. The photographs in **Figure 7(b)** visualize the result of treatment, being almost a full fading of IA loss. This effect can be quantified by a shift of wavelength's transmission, measured at a 3 dB level (see gray line in **Figure 7(a)**), from near-

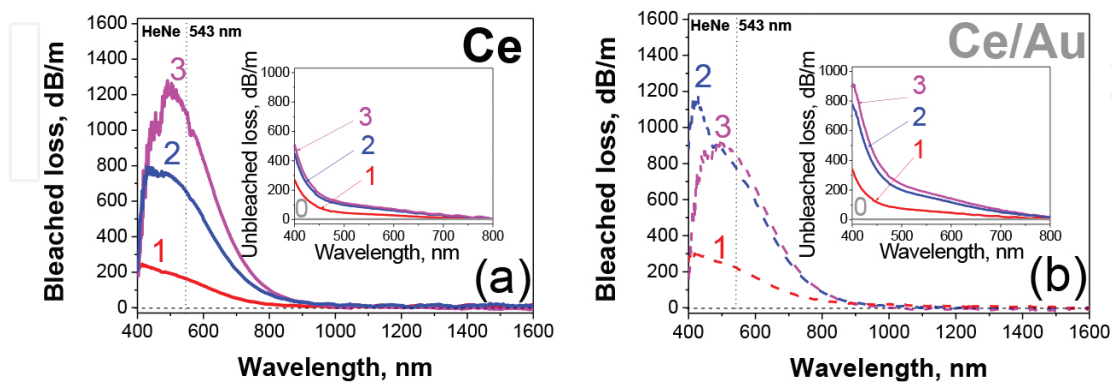


Figure 6. Bleached (main frames) and unbleached (insets) spectral loss in Ce-doped (a) and Ce/Au-codoped (b) fibers after ~0.5 mW 543 nm treatment, posterior to β -irradiation with doses 2 (curves 1), 4 (curves 2), and 6 (curves 3). For comparison, curves 0 demonstrate the attenuation spectra of pristine fibers. (Reproduced with permission from Kir'yakov et al. [75]. Copyright© 2014, Optical Society of America).

IR to VIS. It is seen from **Figure 7(c)**, where we demonstrate the results of experiments with Ce/Au-codoped (black open dots) and Ce-doped (gray open squares) fibers, that it has a similar character for both fibers.

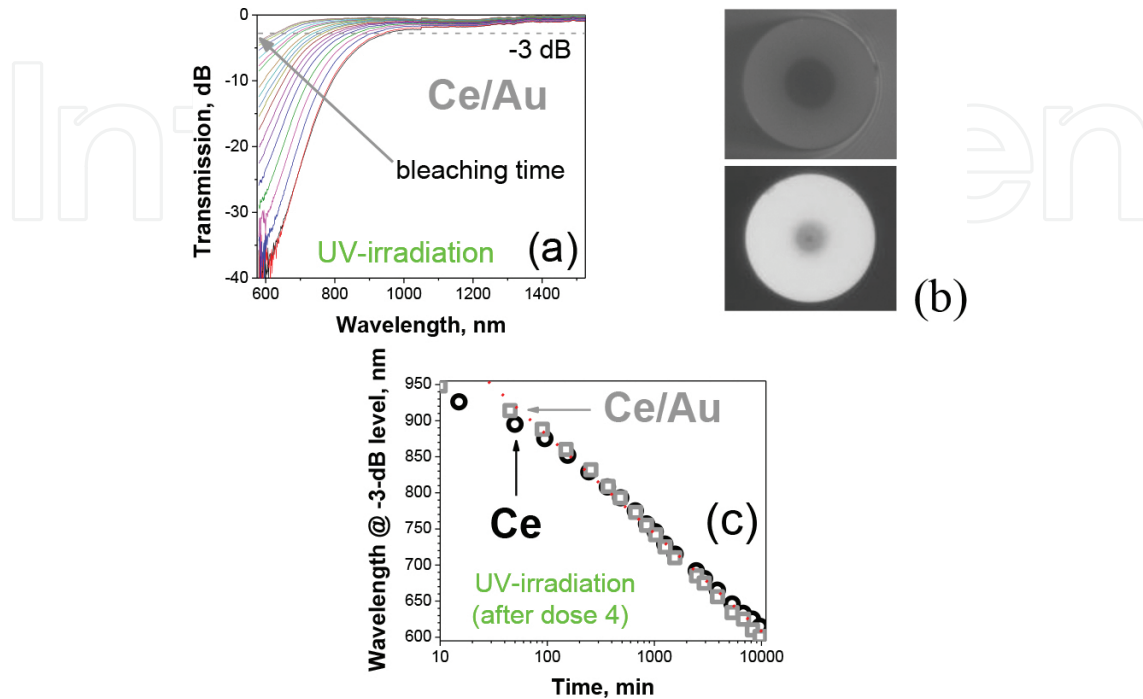


Figure 7. (a) Dynamics of attenuation decay (in terms of transmission of Ce/Au-codoped fiber under UV-lamp illumination with maximal spectral power @350 nm). Bleaching was realized in the darkened fiber, posterior to β -irradiation with dose 4. (b) Micro-photographs of darkened (dose 5 of β -irradiation) Ce/Au-codoped prior to optical bleaching with UV-lamp (top) and after continuous bleaching during 10,000 h (bottom). (c) Examples of the spectral transformations during UV-bleaching in terms of shifting of the fiber's transmission edge wavelength measured at -3 dB level; the data were obtained for Ce/Au-codoped (open black dots) and Ce-doped (open grey squares) fibers, preliminary β -irradiated with dose 4; both the data are fitted to the eye by dotted red lines. (Reproduced with permission from Kir'yanov et al. [75]. Copyright© 2014, Optical Society of America).

2.3. Discussion

2.3.1. Pristine fibers

Regarding pristine Ce-doped and Ce/Au-codoped fibers (**Figure 1**), apart from a strong growth of absorption seen at shorter (VIS to UV) wavelengths (apparently connected with the presence of Ce in valences $\text{Ce}^{3+}/\text{Ce}^{4+}$ [23, 24]), the other two points deserve mentioning, being (i) monotonous growth of loss toward IR in both fibers (of not clear origin but inherent to Ce doping since such trend is absent in the reference Ce free fiber) and (ii) a distinct peak at ~ 520 nm (~ 2.4 eV) in the absorption spectra of both fibers (but absent in the Ce free one). We suppose that this peak has the same origin as band 2 risen at β -irradiation and located at ~ 2.4 eV (see **Figure 4**). This feature has not been reported for bulk Ce-doped silica but is frequently observed in Ce-doped fibers subjected to ionizing radiations [17, 24]. It can be related to quite stable Ce^{3+}h^+ centers, or alternatively while hypothetically, to Ce^{4+}e^- centers (existence of which

was not documented), but apparently not to sole Ce ions being in either trivalent or tetravalent state. As for us, a more realistic cause for the existence of $Ce^{3+}h^+$ or/and $Ce^{4+}e^-$ defect centers in pristine fibers, attributable by the 520 nm peak, can be ionization, that is, generation of electrons e^- and holes h^+ , at the fiber preform's collapse stage [24] or during the fiber's drawing with posterior covering by acrylic outer cladding when—in both situations—strong UV light is produced, with a result being a trapping of free carriers by Ce^{3+}/Ce^{4+} species.

2.3.2. β -irradiated fibers

Consider in more details the results of β -irradiation of Ce-doped and Ce/Au-codoped fibers (**Figures 2–4**). The processes, involved at irradiating the fibers with the result being rise followed by saturation of IA, described by the “stretched-exponent” law [14, 24, 26]), comprise: (i) creating of secondary carriers (holes h^+ and electrons e^-) in the core-glass matrix by β (primary) electrons and their trapping on such glass imperfections as Ce ions (Ce^{3+}/Ce^{4+}), nonbridging oxygen centers, other centers associated with Al and P, and oxygen vacancies; (ii) direct $h^+ \dots e^-$ recombination (annihilation); (iii) thermally or/and radiatively activated recombination between the centers or defects that have arisen during and after β -irradiation. Concerning the role of Ce-doping, we assume that IA is produced via irradiation-induced reactions $Ce^{3+}+h^+ \rightarrow Ce^{3+}h^+ (\rightarrow ?Ce^{4+})$ and $Ce^{4+}+e^- \rightarrow (?Ce^{4+}e^-) \rightarrow Ce^{3+}$ [26–28], implying Ce was in valences 3+/4+ in pristine fibers or/and being generated via irradiation. Note that determination of relative contents of Ce^{3+}/Ce^{4+} ions in the pristine state is hard and that at low Ce doping, mainly fluorescing Ce^{3+} are formed in the core-glass, while at higher overall Ce concentration both Ce^{3+} and Ce^{4+} (nonfluorescing) ions can be present. Unfortunately, the absorption spectra of glasses containing both Ce^{3+}/Ce^{4+} ions have the featuring bands within a 200–400 nm (UV) range (not detectable by our spectral equipment); so any arguing about $Ce^{3+} \leftrightarrow Ce^{4+}$ transformations for this range is impossible. In the meantime, the absorption bands of $Ce^{3+}h^+$ and $Ce^{4+}e^-$ defect centers are expectedly located in VIS (see above), on one hand, and, on the other hand, the detected spectral changes at β -irradiation occur in VIS, too (band 2); thus, formation of metastable centers $Ce^{3+}h^+/Ce^{4+}e^-$ as its result is a worthy proposal.

Furthermore, IA bands 1 (~3.0 eV) and 2 (~2.4 eV) (see **Figure 4**) have been undoubtedly separated; see above. The first of them, in Ce-doped and Ce/Au-codoped fibers, has seemingly the same origin as the one in the Ce-free fiber (see **Figure 2**), that is, it most probably belongs to one, most simply organized, type of the two NBOHCs centers, inherent to silica. The other would stem from Ce doping: it is seen from **Figure 2** that such band does not exist in the reference Ce-free fiber. However, the irradiated Ce-free fiber demonstrates ~600 nm band, probably attributing the other type of NBOHCs [26], absent in both Ce-doped fibers subjected to irradiation: compare spectra 1–3 shown in **Figure 2**. The fact that the dose dependences of IA (**Figure 4**) have different characters for the fibers points on different nature of the centers represented by bands 1 and 2. Therefore, our hypothesis that ~3.0 eV band stems from NBOHCs and that ~2.4 eV one is associated with a Ce-related center ($Ce^{3+}h^+/Ce^{3+}e^-$) seems to be relevant. In our case (alumino-silicate core glass of Ce-doped and Ce/Au-codoped fibers), such “point” defects as Al-E' and Al-oxygen-deficient centers can be also created at trapping secondary

electrons and holes born at β -irradiation (phosphorous (P) presented in small amount plays a little effect).

Thus, the processes roughly schematized as $Ce^{3+} \leftrightarrow Ce^{4+}$ seem to be a sole way to address the spectral transformations seen from Figures 2–4 to happen via the formation in the Ce- and Ce/Au-doped fibers of metastable states Ce^{3+h+}/Ce^{4+e-} . Furthermore, it deserves mentioning that overall susceptibility to β -irradiation (overall IA loss) of Ce-doped fiber is higher than of Ce/Au-codoped one. This may signify that the core glass containing gold is more stable than that solely doped with Ce. On the other hand, deviations in the experimental data for kinetics of IA versus β -irradiation dose for the fibers (refer to IA spectra in **Figure 3** and to dose dependences in **Figure 4**) are more pronounced in the former than in the latter fiber. A possible explanation for this can be that codoping with Au gives rise to the core-glass system more ordered. This property seems to have impact for establishing almost the same path kinetics of defect centers' formation as compared with other factors involved in such of type fibers.

2.3.3. *Optically bleached fibers*

Let us discuss now the effect of partial bleaching of β -irradiated Ce-doped and Ce/Au-codoped fibers under the action of low-power VIS/UV light (see Figures 5–7). Whereas a doubtless conclusion on its nature is hard, some discourse about the matters involved can be made. The processes responsible for recombination of radiation-induced defects or color centers, seen as IA fading (bleaching) of darkened fibers, can be of thermally and/or optically induced origin. Bleaching, with its result being decreasing IA versus time, seems to be an example of mainly optically induced recombination of both types of centers, NBOHCs and Ce-related Ce^{3+h+} (assumed to be represented by bands 1 and 2, respectively) ones.

As seen from **Figure 5(d)** and **Figure 7(c)**, IA decreases almost exponentially at the beginning of bleaching. However, within the whole interval of optical bleaching, IA in bands 1 and 2 is seen to fade (in terms of negative AD at 543 nm illumination, see **Figure 5(a, b)**), as well as in terms of shifting the transmission edge to shorter wavelength, at exposure the fibers to UV light, see **Figure 7(a, c)**), which obeys a “stretched exponent” law [26]. An explanation for this behavior can be not only complexity of the mechanisms involved at optical bleaching but also a fact of limited “penetration” of bleaching light into a fiber sample (especially in the case of 543 nm bleaching).

Concerning the essence of IA at optical bleaching, we can, at the current stage of our knowledge, propose them only tentatively. If our attribution of IA bands 1 and 2 as “signatures” of NBOHCs and Ce-related Ce^{3+h+} centers is correct, then these centers, formed at trapping free holes, should be breaking via the holes' detrapping and annihilating with free electrons born at interaction with VIS/UV light. Weak intensity of bleaching light is guessed to produce mainly extra electrons rather than holes in the core-glass, leading to dominance of the processes relating to the hole-trapped centers, such as NBOHC (~3.0 eV band) and Ce^{3+h+} ones (~2.4 eV band). Note that a strong candidate to be “in-charge” of production of e^- at the UV/VIS excitation may be Ce^{3+} ions themselves [15].

Comparison of the bleaching effect in Ce-doped (without Au codoping) and Ce/Au-codoped fibers show that it is less expressed in the latter than in the former, which is probably related to lower susceptibility to exterior influence of Ce/Au-codoped fiber (a consequence of its more ordered glass network, already noticed).

3. Electron irradiation versus PD of Yb-doped germano-alumino-silicate fibers: The effects comparison

Yb³⁺-doped silica fibers (YFs) with different core-glass hosts codoped with Al, Ge, or P have been of considerable interest during the past decades as extremely effective media for fiber lasers for the spectral region 1.0–1.1 μm, when pumped at 0.9–1.0 μm wavelengths. A variety of diode-pumping configurations (core and cladding) and pump wavelengths were examined so far, resulting in recognition of optimal arrangements for multi-watt release from YF-based lasers with high optical efficiency ~70–75% and perfect beam quality [29, 30]. However, in spite of a remarkable progress in the field, there remain obstacles that limit the performance of YF-based lasers, one of them being PD [31], that is, long-term (minutes to hours) degradation of laser power, measured by units to tens %. This hardly mitigated disadvantage becomes notable when dealing with a laser based on heavily doped YF where a high Yb³⁺ population inversion is created, either at high-power continuous-wave or moderate-power pulsed lasing. A number of studies were aimed to understand the PD phenomenon which however remained unclear, although a few hypotheses have been proposed for its explanation [32–42].

On the other hand, a few studies aiming the characterization of susceptibility of YFs under such irradiations as X-rays, γ-quanta, and UV have been reported [43–45]. The main motivation was inspection of YF-resistance to harmful environments. In many cases, the excess-loss spectra induced in YFs resemble the ones, characteristic for PD at resonant pumping into Yb³⁺ resonant-absorption band, the fact undoubtedly deserving attention.

Here, the results of two sets of experiments, where susceptibility of YFs with similar germano-alumino-silicate glass-cores, doped with Yb in different concentrations to irradiation by a beam of β-electrons and to resonant (into Yb³⁺ resonant band) optical pumping, are presented. In both circumstances, qualitatively similar trends are revealed, being strong and monotonous change in attenuation in VIS (darkening), accompanied by more complex transformations within the resonant absorption band of Yb³⁺ ions, either upon dose (the case of β-electron irradiation), or exposing time (the case of optical pumping at 977 nm). Below, we compare and discuss the experimental results and attempt to explain them.

3.1. Fiber samples and experimental arrangement

The YFs inspected in these experiments were drawn from germano-alumino-silicate glass preforms fabricated using the “conventional” MCVD/SD route. The attenuation spectra of the fibers being in pristine (as-received) state are demonstrated in **Figure 8(a)**.

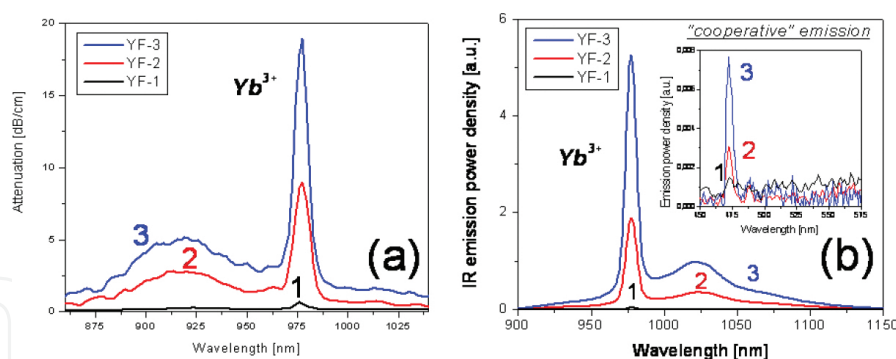


Figure 8. (a) Attenuation (small-signal absorption) spectra of fibers with low (YF-1), intermediate (YF-2), and high (YF-3) Yb^{3+} contents: curves 1, 2, and 3, respectively. (b) Fluorescence spectra of the fibers at resonant 977 nm excitation (pump power—300 mW). Labeling of curves 1, 2, and 3 is the same as in (a) and (b). Inset in (b) shows “cooperative” fluorescence in VIS. (Reproduced with permission from Kir’yanov [76]. Copyright© 2011, Scientific Research Publishing Inc).

The concentrations of Yb^{3+} ions in the fibers differed by more than an order of magnitude, so certain differences were expected after their exposure to β -electron irradiation (hereafter in this paragraph—*e-irradiation*) and to optical pumping (hereafter—*OP*) at 977 nm wavelength. The fibers, having the lowest, the intermediate, and the highest Yb^{3+} doping level, are referred further to as *YF-1*, *YF-2*, and *YF-3*, respectively.

The essences of experiments on *e-irradiation* of the YFs were completely the same as at irradiating the Ce-doped fibers (Paragraph 2). The indices “1,” “2,” and “3” label below the doses 2×10^{12} , 1×10^{13} , and $5 \times 10^{13} \text{ cm}^{-2}$, respectively.

Experiments on *OP* at 977 nm were made in a similar way as described in Ref. [36]. YF samples were pumped using a standard 300 mW 977 nm laser diode (LD). The pump light was launched from LD to an YF sample under study through a splice. The end of the latter was spliced to a piece of SMF-28 fiber that was, in turn, connected to an OSA for the transmission spectra’ measurements. In these experiments, we handled short (a few cm) pieces of YFs to ensure non-lasing conditions and negligible contribution of amplified spontaneous emission of Yb^{3+} .

The optical transmission spectra of the YF samples were obtained using a white light source with a fiber output and the OSA, turned to a 1 nm resolution. These spectra were recorded over the spectral range 400–1200 nm, where the most interesting spectral transformations occur as the result of *e-irradiation/OP*. The output of the white light source was connected to a fiber set containing an YF sample (pristine or subjected to *e-irradiation/OP*), while its attenuation was measured using the OSA. The attenuation spectra were recorded before and after each stage of *e-irradiation* (*doses*) or *OP* at 977 nm pumping (*times*). Lengths of the YFs were chosen to be short enough, from <1 cm (YF-3) to tens cm (YF-1), to avoid spectral noise artifacts. In some of the figures below, the difference (IA) spectra are demonstrated which were obtained after subtracting the attenuation spectra of pristine samples from the ones taken after certain dose/time of *e-irradiation/OP*. This allows insight to “net” spectral loss, established after darkening of either type. All the spectra presented beneath have been obtained after recalculating transmission coefficients in loss [dB/cm]. We also measured the fibers’ fluorescence

spectra and fluorescence kinetics of Yb^{3+} ions before and after e-irradiation/OP, applying the “lateral” geometry [46]. We used the same OSA for the fluorescence spectra measurements and a Ge photodetector (PD) and oscilloscope for the fluorescence-decay measurements. In the last case, LD power was modulated by a driver controlled by a function generator to achieve square-shaped pulses with sharp rise and fall edges. The time resolution of the setup was 8 μs . All the experiments were made at room temperature.

3.2. Experimental

3.2.1. E-irradiation

The attenuation spectra of samples YF-3 and YF-1, having correspondingly the highest and lowest Yb^{3+} concentrations, obtained after different doses of e-irradiation, along with the attenuation spectra of the samples in a pristine (dose “0”) state are shown in **Figure 9(a, b)**.

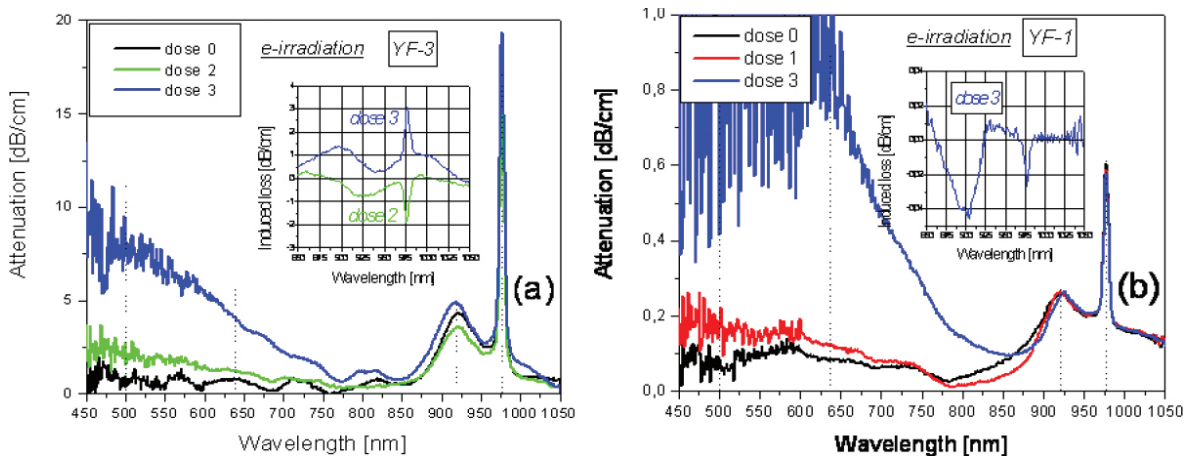


Figure 9. Attenuation spectra of samples YF-3 (a) and YF-1 (b). The data are for e-irradiation doses increased from “0” (pristine samples) through “1” and “2”–“3”. Insets show the difference spectra obtained after subtraction of the spectra of pristine samples from the ones after e-irradiation of the samples. Dashed lines show the positions of wavelengths for which the data in **Figure 10** are built. (Reproduced with permission from Kir’yanov [76]. Copyright© 2011, Scientific Research Publishing Inc).

First, a notable increase of background loss in VIS with increasing e-irradiation dose is revealed (see main frames of **Figure 9**). Also notice a specific spectral character of this loss for both fibers, viz. a drastic rise of loss-magnitude toward shorter wavelengths. This is a well-known for Yb^{3+} -free silica fibers’ trend in experiments on various kinds of irradiations. At the same time, apparent differences are seen in magnitude of e-irradiation-induced loss in these two fibers, that is, a higher degree of darkening in YF-3 than in YF-1. (For YF-2, intermediate in Yb^{3+} doping level, the effect of e-irradiation is intermediate, as compared with YF-3 and YF-1.)

Second, detectable but less pronounced spectral transformations are revealed for the resonant-absorption band of Yb^{3+} (850–1100 nm) (see insets to **Figure 9**), where the difference spectra

are shown, obtained as explained above. Very weak in YF-1 (Figure 9(b)), the spectral transformations are noticeable in YF-3 (Figure 2(a)). These changes seem to be a result of some process, associated with e-irradiation of the fibers, which affects concentration of Yb^{3+} ions.

More details are seen in **Figure 10** where we plot the results for samples YF-1 (a) and YF-3 (b), taken for all doses. **Figure 10(a, b)** demonstrates how attenuation within the resonant-absorption of Yb^{3+} ions (peaks at 920 and 977 nm, see also **Figure 8(a)**) changes throughout e-irradiation: see curve 1 (for the 977 nm peak) and curve 2 (for the 920 nm peak), respectively. A decrease followed by an increase in the magnitude of small-signal absorption arises in both peaks with dose increasing in YF-3 (heavier doped with Yb^{3+}); this trend is, in contrast, less expressed in YF-1 (lower doped with Yb^{3+}).

For comparison, we plot in **Figure 10** the changes in attenuation of YF-3 (c) and YF-1 (d) fibers in VIS, where background (nonresonant) losses arise as the result of e-irradiation. Here we limit ourselves by the data, counted for 500 (curve 3) and 633 (curve 4) nm. It is seen that background loss steadily grows with dose, a common effect for silica fibers. Note that the rate of growth is higher in YF-3 than in YF-1. Furthermore, an initial level of background loss in pristine YF correlates with initial content of Yb^{3+} ions.

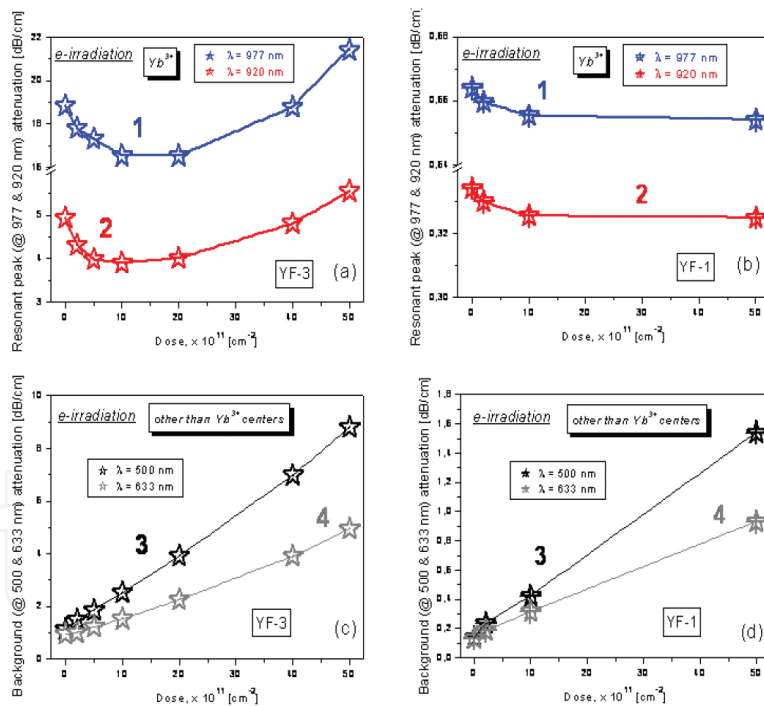


Figure 10. Dose dependences of attenuation in resonant-absorption Yb^{3+} peaks centered at 977 (curves 1) and 920 (curves 2) nm (top panels) and in VIS, for wavelengths 500 (curves 3) and 633 (curves 4) nm (bottom panels). The data are for samples YF-3 (a, c) and YF-1 (b, d). (Reproduced with permission from Kir'yanov [76]. Copyright© 2011, Scientific Research Publishing Inc).

Figure 11(a) and **(b)** gathers the experimental data obtained using all fibers, YF-1, YF2, and YF-3. From **Figure 11(a)**, it is seen that a monotonous increase of nonresonant loss in VIS (darkening), exemplified by wavelengths 500 and 633 nm, with increasing Yb^{3+} concentration;

the latter is proportional to YF small-signal absorption at 977 nm. This demonstrates that the presence of Yb^{3+} dopants gain their degradation at e-irradiation. (Here we show the results obtained at dose "3" only, because for other doses the dependences are similar, given by a smooth dependence of induced loss in VIS versus e-irradiation dose (see **Figure 10(c, d)**). From **Figure 11(b)**, it is seen that the lowest levels to which the values of absorption in the 977 nm peak approach throughout e-irradiation (minima of curves 1 in **Figure 9**) decrease with increasing Yb^{3+} content (a similar trend is observed for the other peak of Yb^{3+} , at 920 nm). This fact seems to be in favor of that initial concentration of Yb^{3+} ions in pristine samples substantially decreases as a result of e-irradiation, at the primary stage. However, at the following stages, Yb^{3+} concentrations are re-established on levels comparable with those in pristine YFs (refer to **Figure 10(a)**). [The remainder of **Figure 11(c, d)** provides the data, obtained in the experiments on OP of the YFs, reported below.]

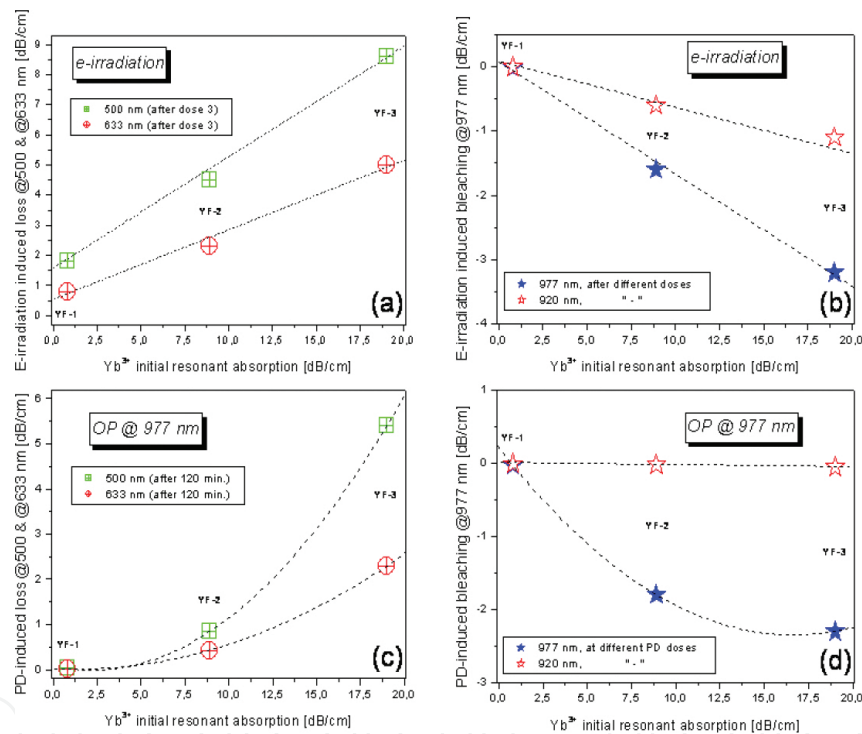


Figure 11. The results of experiments with fibers YF-1, YF-2, and YF-3, which were obtained for different e-irradiation doses (a, b) and OP times (c, d). The data are for the resonant-absorption peaks at 977 and 920 nm (filled and empty asterisks) (b, d) and for the VIS region, exemplified by wavelengths 500 nm (crossed squares) and 633 nm (crossed circles) (a, c). Dotted lines are for visual purposes only. (Reproduced with permission from Kir'yakov [76]. Copyright© 2011, Scientific Research Publishing Inc).

3.2.2. PD at OP

We report here the results of OP experiments for sample YF-3 mainly (see **Figures 12–14**), having the biggest content of Yb^{3+} ions. Then, we summarize all the results, obtained for YF-1, YF-2, and YF-3 fibers, in **Figure 11(c, d)**.

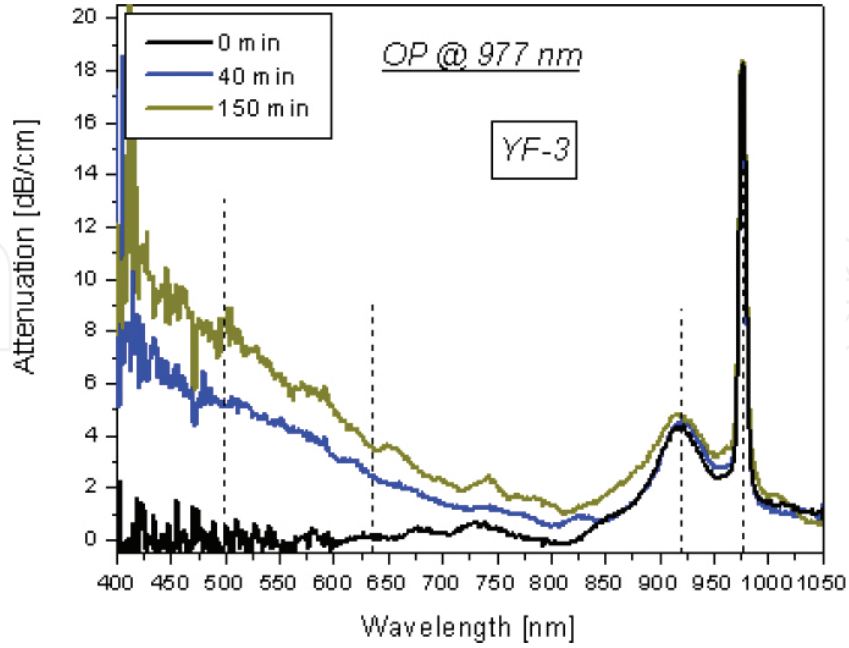


Figure 12. Attenuation (small-signal absorption) spectra of fiber sample YF-3 after OP @ 977 nm. The data are for a pristine sample (curve 1: “0 min”) and for photo darkened samples (curves 2 and 3, obtained after 40 and 150 min of OP, respectively). Dashed lines show the positions of wavelengths for which the data in **Figure 13** are built. (Reproduced with permission from Kir’yanov [76]. Copyright© 2011, Scientific Research Publishing Inc).

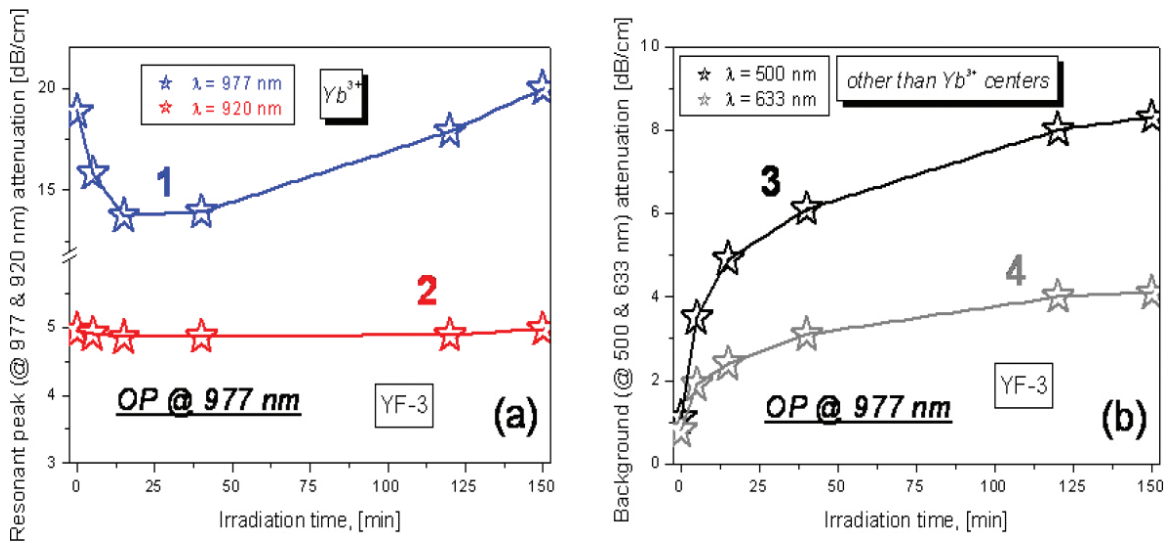


Figure 13. Dose dependences of attenuation in resonant-absorption (Yb^{3+}) peaks centered at 977 (curve 1) and 920 (curve 2) nm (a) and in VIS, for wavelengths 500 (curve 3) and 633 (curve 4) nm (b). The data are for sample YF-3. (Reproduced with permission from Kir’yanov [76]. Copyright© 2011, Scientific Research Publishing Inc).

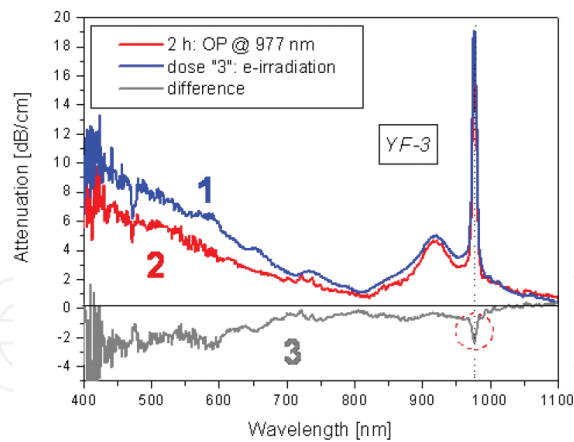


Figure 14. Difference attenuation spectra after dose “3” of e-irradiation (curve 1) and after 2 h of OP at 977 nm (pump power is 300 mW) (curve 2); curve 3 is the difference of spectra 1 and 2. The data are for sample YF-3. (Reproduced with permission from Kir’yanov [76]. Copyright© 2011, Scientific Research Publishing Inc).

Figure 12 shows the attenuation spectra of sample YF-3 (length, 0.8 cm) after 40 and 120 min. of OP. The LD power was fixed in these experiments at 300 mW, the highest in our circumstances level of Yb^{3+} ions inversion. For comparison, the attenuation spectrum of pristine (0 min) sample YF-3 is shown in **Figure 12**, too. Once compared with the attenuation spectra after e-irradiation (refer to **Figure 9(a)**), these spectra are seen to be similar. That is, a substantial increase of background loss is observed in VIS with increasing OP-time (the PD effect). Note that the spectral “signature” of PD resembles the one after e-darkening (see **Figure 9**).

In **Figure 13(a)**, we demonstrate the results of the experiments with sample YF-3, obtained at increasing OP time. Their representation is similar to the one used at the description of experiments on e-irradiation (see **Figure 10(a)**). From **Figure 13(a)**, it is seen how attenuations in the two absorption peaks of Yb^{3+} ions (at 977 and 920 nm) change throughout OP; see curves 1 and 2, respectively. The time dependence of OP-induced changes at 977 nm resembles the dose dependence at e-irradiation of sample YF-3. However, curve 1 in **Figure 13(a)** has “asymmetric” shape versus OP time, differing from “symmetric” shape of the dose dependence at e-irradiation given by curve 1 in **Figure 10(a)**. Furthermore, the time dependence of OP-induced changes at 920 nm, see curve 2 in **Figure 13(a)**, is very weak, being completely different from curve 2 in **Figure 10(a)** (e-irradiation). Therefore, we can propose that different mechanisms, responsible for the induced changes in the resonant-absorption band of Yb^{3+} at 977 and 920 nm, stand behind these two (e-irradiation and OP) treatments of the fibers.

In **Figure 13(b)**, we demonstrate the results of spectral transformations arising in YF-3 in VIS, at OP. Again, we provide in **Figure 13(b)**, the data for a couple of wavelengths, 500 (curves 3) and 633 (curves 4) nm, as most representative. In contrast to the dose dependences at e-irradiation, long-term OP at 977 nm results in completely different dynamics of background loss in time. Indeed, it is essentially nonlinear versus time: there is a short timing interval in the beginning (few minutes) where PD increases dramatically, while afterward (tens of minutes) it slows down and tends to saturate.

Figure 14 allows one to compare the attenuation spectra for YF-3 suffered dose “3” of e-irradiation (curve 1) and 2 h of OP (curve 2). The spectra look qualitatively similar, which may tell that the mechanisms involved are similar in these two circumstances. At the same time, if one spectrum is subtracted from another, the result (curve 3 in **Figure 14**) brings some news. That is, apart from the difference presented in VIS (in background loss), there is a feature in the Yb^{3+} resonant band: though no deviation from “plain” behavior of curve 3 is seen near 920 nm peak of Yb^{3+} , there is a well-defined (negative) 977 nm peak (it is marked by a dotted ring). This detail seems to be important as it lightens nonhomogeneity within the Yb^{3+} resonant-absorption band near 977 nm, present at OP but not—at e-irradiation.

This detail becomes expressed more when one analyzes the data obtained at PD of the other fibers, YF-1 and YF-2 (see **Figure 15**). In this figure, where we plot the difference spectra obtained for these fibers, analogous but clearer seen detail appears exactly within the 977 nm peak of Yb^{3+} ions (it is marked by a dotted ring in (a) and (b)).

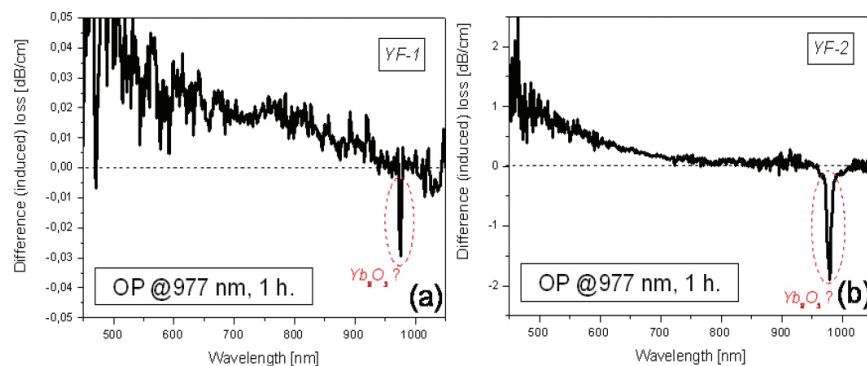


Figure 15. Difference loss spectra of YF-1 (a) and YF-2 (b), obtained after 1 h of OP at 977 nm. (Reproduced with permission from Kir’yanov [76]. Copyright© 2011, Scientific Research Publishing Inc).

Let us return to **Figure 11(c, d)**, where we gather the results on OP for all YF samples.

In contrast to the results on e-irradiation (**Figure 11(a, b)**), one can reveal first nonlinear growth of background loss at 500 and 633 nm with increasing Yb^{3+} concentration (**Figure 11(c)**). Apparently, this behavior is different from linear growth of background loss at e-irradiation (**Figure 11(a)**). Second, it is seen that, instead of a linear decrease of the resonant peaks at 977 and 920 nm with dose (occurring at primary stages of e-irradiation—see **Figure 11(b)**), a nonlinear law is obeyed by a decrease of the resonant peak at 977 nm while almost no change happens with the peak at 920 nm (**Figure 11(d)**).

Thus, the situation with OP-induced spectral transformations in the YFs is complex and curious at first glance. The 977 nm peak is strongly affected by OP, not the 920 nm one. This can be explained by the presence in the fibers of some other centers than Yb^{3+} dopants, but closely related to them and spectrally matching them near 977 nm. Moreover, partial weight of such centers in YF-core is expected to increase with increasing Yb^{3+} ions concentration. The nonlinear behavior of the nonresonant background loss versus OP time, discussed earlier (see **Figure 13(b)**), seems to be a related phenomenon.

3.2.3. What's about fluorescence?

The fluorescence spectra obtained using pristine YF-1, YF-2, and YF-3 fibers at 977 nm pumping are shown in **Figure 8(b)**. All these are similar in appearance and their intensities are proportional to Yb³⁺ ions concentrations in the fibers (The measurements were made at the same conditions and at the same pumps.)

We also measured the fluorescence spectra of the YFs after irradiation by an electron beam and after long-term OP at 977 nm, but almost no qualitative spectral changes were captured in the Yb³⁺ fluorescence band; so we don't provide them here. We could only notice a small decrease in the fluorescence power as the result of the treatment, but this trend could not be quantified. Furthermore, it was found that the characteristic Yb³⁺ fluorescence decay time slightly decreases in the set of pristine YFs. This is a result of the presence of two exponents in the fluorescence kinetics, measured by ~0.7 and ~0.2...0.3 ms. Note that insignificant growth of the latter contribution was detected for the fiber with the highest Yb³⁺ content (YF-3); see also Ref. [46–48]. However, the time constants obtained at fitting were nonaffected neither by e-irradiation nor by long-term OP. Concluding, we can reveal that none, or very insignificant, changes occurred in the YFs in the sense of Yb³⁺ fluorescence.

3.3. Discussion

Summarizing all the data, we notice that either at e-irradiation or at resonant OP substantial and complex but different in appearance changes arise within the resonant absorption band of Yb³⁺ ions (“reversible bleaching”), while monotonous growth of nonresonant background loss is observed in VIS (“darkening”). Furthermore, these trends are revealed to stem from the changes in concentrations of Yb³⁺ ions and, seemingly, of other centers, closely related to them and spectrally matching them near 977 nm. This is the main news of this study.

A general consequence of the experiments on e-irradiation, rise of background nonresonant loss in YFs in VIS (see **Figure 10 (c, d)**), is not surprising. This loss correlates spectrally with the excess loss arising in optical fibers at other types of irradiation (X-rays, γ -quanta, UV [33–35]). Some other aspects are as follows:

1. A monotonic increase of the background loss in VIS (darkening) with increasing Yb³⁺ content in the YFs, which demonstrates that the presence of Yb³⁺ dopants leads to a higher degree of the fibers' degradation at e-irradiation (**Figure 11(a)**).
2. A notable decrease followed by equally notable increase arising in the resonant-absorption peaks of Yb³⁺ (at 920 and 977 nm) with increasing e-irradiation dose (**Figure 10 (a, b)**), the effect also dependent on Yb³⁺ concentration (**Figure 11(b)**).

Thus, the presence of Yb³⁺ dopants in the fibers results in a more pronounceable degradation at e-irradiation, with a probable reason being that Yb³⁺ ions are powerful sources of secondary carriers (electrons and holes) born at e-irradiation. That is, the changes within the resonant-absorption band of Yb³⁺ may stem from excitation of inner-shell (*f*) electrons of Yb³⁺ and their valence transformation through the charge-transfer (CT) processes (direct and reversed), sketched by the following reactions [36]: $e^- + Yb^{3+} \rightarrow Yb^{2+}$; $e^+ + Yb^{2+} \rightarrow Yb^{3+}$,

where e^- and e^+ stand for secondary (irradiation induced) electrons and holes, and Yb^{2+} is the notation for Yb ions in 2+ valence state. In turn, the presence in the fibers of secondary carriers as the result of e-irradiation can produce such defects as oxygen-deficit center (ODC) and NBOH centers [47]. These centers are known to be responsible for the wide excess-loss spectral bands similar to the ones produced in the darkened fibers (**Figures 9 and 14**).

Qualitatively similar observations can be made regarding the spectral transformations in the YFs as the result of OP at 977 nm (refer to **Figure 11(c, d)** and **Figures 12–15**). Analogously, the following trends are drawn:

3. Background loss in VIS substantially grows at long-term OP (see **Figures 12 and 13(b)**) while its character is typical for PD in YFs [31–41]. However, an increase of this loss in VIS with increasing small-signal absorption has, in contrast to e-irradiation, a nonlinear law (**Figure 11(c)**), thus revealing an almost quadratic dependence versus Yb^{3+} concentration.
4. The dependences of resonant absorption, measured in the peaks of Yb^{3+} at 977 and 920 nm upon OP time, have essentially different characters (**Figure 13(a)**). If the absorption coefficient in the 977 nm peak changes by a law similar to the one at e-irradiation, the absorption coefficient in the 920 nm peak is virtually constant throughout long-term OP. The concentration dependences shown in **Figure 11(d)** tell us more: the changes in these peaks with increasing content of Yb^{3+} ions are also different. We cannot interpret these details in terms of simple concentration dependences in regard to Yb^{3+} ions. Otherwise, an assumption can be made instead that the changes in the 977 nm peak are related to the changes in concentration of some others than Yb^{3+} ions centers but spectrally matching them in the 977 nm peak.
5. The spectral signature of the latter is seen from **Figures 14 and 15** where the difference attenuation spectra after OP are demonstrated. One can see from these figures that the PD effect (growth of nonresonant loss in VIS) is accompanied by bleaching of the resonant peak at 977 nm, whereas none happens with the peak at 920 nm. Note that a similar feature was reported earlier for the other type of YF, fabricated by the DND method [36].

The observations (3–5), when gathered together, tell us that PD in the YFs at high-power, long-term OP at 977 nm arises among the centers concentration of which is a nonlinear (almost quadratic) function of Yb^{3+} ions concentration. These are most probably the centers composed of couples of Yb^{3+} ions (*pairs*), or agglomerates of the latter. Furthermore, similar reactions: $e^- + Yb_p^{3+} \rightarrow Yb_p^{2+}$; $e^+ + Yb_p^{2+} \rightarrow Yb_p^{3+}$ (see above) can be proposed to address these transformations at OP, where index p stands to show that a pair of Yb^{3+} ions is involved in the processes and notations e^- and e^+ are used for an electron and a hole, free or trapped by the nearest ligand, say oxygen. Such reactions can go at the assistance of CT-processes between ion pairs where both constituents are in the excited state. Hence, the spectrally wide background loss (PD) in the fibers (see **Figures 12 and 14**) can be produced Yb_p^{2+} and of e^-/e^+ -related centers (say, ODCs and NBOHCs) at OP, like this takes place at e-irradiation.

It is currently accepted that PD occurs among clusters of Yb^{3+} ions (obviously, pairs are their kind). However, a novelty found here is the spectral feature, occurring at OP (see dotted rings in **Figures 14** and **15**) but not—at e-irradiation.

There are evidences for that PD can be itself associated with nonbinding oxygen near surfaces of Yb/Al clusters that can be formed in alumino-silicate glass (our case). The nonbinding oxygen originates from Yb^{3+} substituting Si^{4+} sites. When subjecting a YF to 977 nm OP, the excess energy is radiated as phonons, causing a lone electron of a nonbinding oxygen atom to shift to a nearest neighbor nonbinding oxygen atom with creation of a hole and a pair of lone electrons, which results in a Coulomb field between the oxygen atoms to form an unstable “color” center. Conversion of such an unstable center to a semistable center requires shifting of one electron of the lone electron pair to a nearest neighbor site. As a result of this, the formation of Yb-related ODC can happen. On the other hand, PD in alumino-silicate YFs may take place via breaking of ODC, which gives rise to release of free electrons. The released electrons may be trapped at Al or Yb sites to form a color center resulting in PD. These hypotheses can serve as the arguments, bringing more clarity in understanding the similarity of the spectral transformations in YFs at e-irradiation (creation of “secondary” carriers by β -electrons) and at OP (creation of carriers and color centers by pump-light).

4. Effect of electron irradiation upon optical properties of Bi-doped silica fibers

Bi-doped silica fibers with core-glass codoped with Al, Ge, or P are currently of increasing interest, being a promising active medium for amplifying and lasing in the spectral range 1.1–1.6 μm (see e.g. [49–59]). In spite of remarkable success in the field, there remain certain obstacles for further improvements of Bi fiber lasers and amplifiers because the main problem is lack of clarity in the nature of Bi “active” centers (Further—BACs) in silica glass. Thus, any research aiming to recover the essences of BACs would have value.

Below we highlight the effect of irradiation of Bi-doped germano- and alumino-silicate fibers by a beam of free electrons of high energy. The main result of the treatment was found to be decrement (“bleaching”)/increment (rise of resonant absorption) in the characteristic peaks, being ascribed to BACs in Bi-doped germano-silicate/alumino-silicate fibers. (Note that analogous trends were reported for similar fibers and glasses under the action of UV laser pulses and γ -quanta [60, 61]). Given that the other optical properties of the fibers under scope, such as BACs fluorescence spectra and lifetimes, were found to be weakly affected by electron irradiation, the changes in the absorption spectra should be associated with the changes in BACs concentration, as firmly justified in our study.

4.1. Fiber samples and experimental arrangement

The Bi-doped silica fibers were drawn from Ge and Al codoped silicate-glass preforms, fabricated applying the MCVD/SD technique. Core radii of the fibers were measured to be in the 2...3 μm range. The representative attenuation spectra of pristine (as-received) Bi-doped

germano- and alumino-silicate fibers, having comparable contents of BACs, are shown in **Figure 16**. Hereafter, the emission-active BACs are referred to as Bi(Ge,Si) and Bi(Al), respectively, in these two types of fiber. Impact of electron irradiation on the basic characteristics of the fibers, referred to further as *Bi-1*, *Bi-2*, and *Bi-3* (germano-silicate) and *Bi-4* (alumino-silicate), is addressed subsequently.

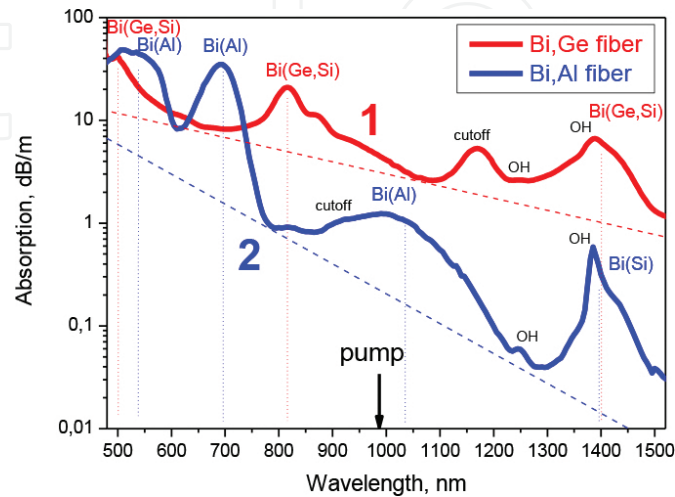


Figure 16. Attenuation spectra of typical Bi-doped germano-silicate (curve 1) and alumino-silicate (curve 2) silica fibers. Arrow shows the pump wavelength (977 nm) used in the experiments on fluorescence spectra and lifetimes measurements. Dashed lines show schematically a trend of the background loss to grow toward shorter wavelengths. (Reproduced with permission from Kir'yanov [67]. Copyright© 2011, Optical Society of America).

Electron irradiation of Bi-1...Bi-4 fibers was proceeding in the conditions, described in Introduction; the indices "1," "2," and "3" label to doses 2×10^{12} , 1×10^{13} , and 5×10^{13} cm⁻², respectively. The technique applied to reveal the spectral transformations in attenuation of the Bi-doped fibers as the result of irradiation was completely the same as described in Paragraphs 2 and 3 and is not repeated here. When measuring Bi-related fluorescence, we utilized the same LD (pump wavelength, 977 nm) for excitation. As seen from **Figure 16**, the pump wavelength was on the Stokes tail of the 750–950 nm absorption band of BACs in Bi-doped germano-silicate fiber and, correspondingly, on the anti-Stokes slope of the absorption band (centered at 1050 nm) of BACs in Bi-doped alumino-silicate fiber. We applied in the BACs fluorescence measurements the lateral detecting geometry, when it was collected from the surface of a Bi-doped fiber sample; the same OSA and a Ge PD were handled to proceed the fluorescence measurements.

4.2. Experimental

The experimental results are presented by **Figures 17–21**. The attenuation spectra of Bi-doped germano-silicate fiber sample Bi-2 subjected to electron irradiation with doses "2" and "3" are shown in **Figure 17(a)** along with the attenuation spectrum of a pristine (dose "0") fiber of the same type. A strong irradiation-induced bleaching effect can be revealed from the figure, seen as drop of magnitude of the absorption peaks labeled "1" (the 750–950 nm band) and "2" (the

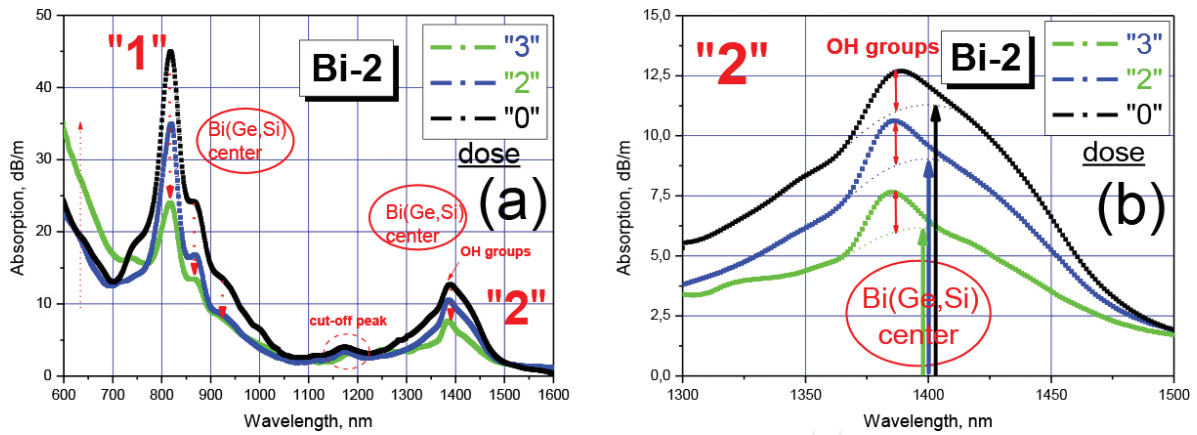


Figure 17. (a) Attenuation spectra of Bi-doped germano-silicate fiber sample Bi-2 obtained before (dose "0") and after (doses "2" and "3") irradiation. The spectral area, comprising the resonant-absorption peaks "1" and "2" which attribute Bi(Ge,Si) centers in the host glass, is shown (b) Insight to the spectral area of peak "2" in a vaster scale. (Reproduced with permission from Kir'yanov [67]. Copyright© 2011, Optical Society of America).

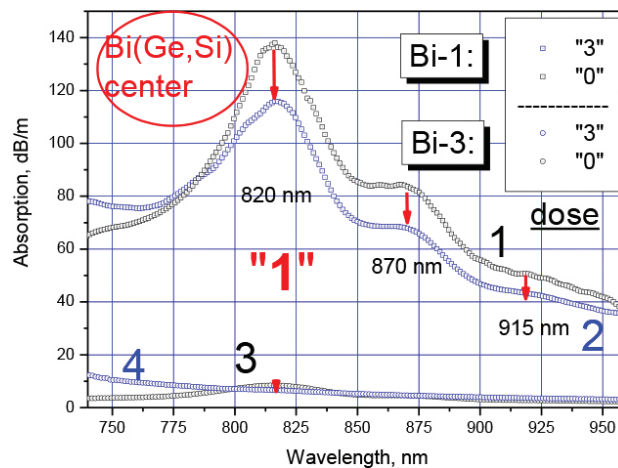


Figure 18. Attenuation spectra of Bi-doped germano-silicate fibers Bi-1 (curves 1 and 2) and Bi-3 (curves 3 and 4), obtained before (dose "0") and after (dose "3") electron irradiation. [The spectral area for the peak "1" is zoomed.] (Reproduced with permission from Kir'yanov [67]. Copyright© 2011, Optical Society of America).

1250–1450 nm band). It is accompanied by an increase of background loss at shorter wavelengths (refer to the left side of **Figure 17(a)**), a well-known feature in experiments on influence of various type of irradiations on optical properties of Ge-doped silica fibers (see e.g. Refs. [62–66]). Unfortunately, such a drastic growth of background loss did not allow us to make well-resolved measurements of the irradiation-induced transformations of BACs band peaked at ~500 nm (see **Figure 16**), so we inspected mostly the changes in peaks "1" and "2". Also notice that almost no changes arise in the attenuation peak at 1180 nm, which corresponds to the cutoff wavelength: this and other Bi-doped germano-silicate fiber samples were drawn to provide single-mode propagation for wavelengths >1200 nm.

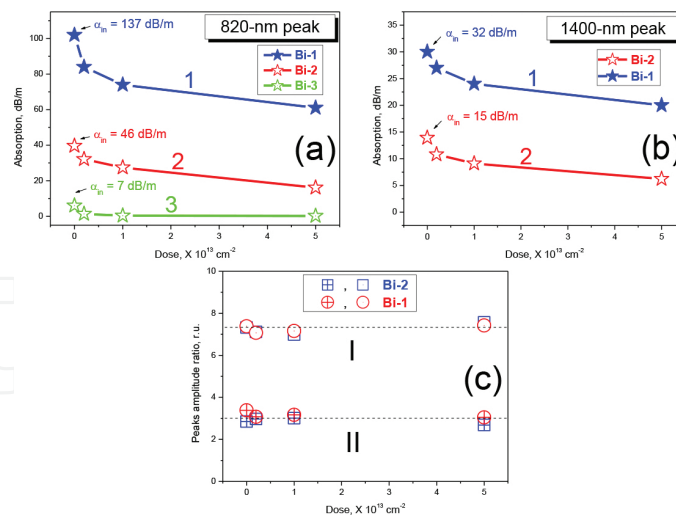


Figure 19. Dose dependences of attenuation of the resonant-absorption peaks “1” (~820 nm) (a) and “2” (~1400 nm) (b): The data for Bi-1 (curves 1), Bi-2 (curves 2), and Bi-3 (curve 3) are shown. (c) insights dose dependences of the peaks magnitudes’ ratios (820...1400 nm – curve I and 500...1400 nm – curve II), for fibers Bi-1 (circles) and Bi-2 (squares). (Reproduced with permission from Kir’yanov [67]. Copyright© 2011, Optical Society of America).

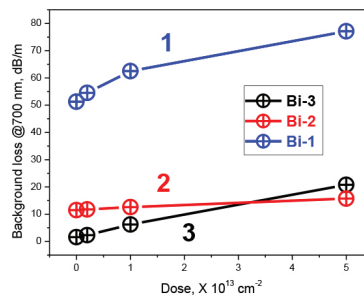


Figure 20. Dose dependences of background loss measured at 700 nm for fibers Bi-1 (1), Bi-2 (2), and Bi-3 (3). (Reproduced with permission from Kir’yanov [67]. Copyright© 2011, Optical Society of America).

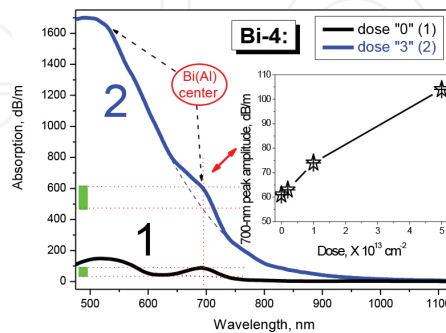


Figure 21. Attenuation spectra of Bi-doped alumino-silicate fiber Bi-4, obtained before (curve 1, dose “0”) and after (curve 2, dose “3”) electron irradiation. A part of the spectra is shown where the main resonant-absorption peaks of Bi(Al) centers are observed. Inset highlights the behavior of one of the peaks (at ~700 nm) against the irradiation dose. (Reproduced with permission from Kir’yanov [67]. Copyright© 2011, Optical Society of America).

Of separate interest is the behavior of absorption peak “2.” Since absorption of BACs in this spectral area is covered by an absorption peak of OH groups (1385 nm), we found reasonable to zoom the spectral transformations for this range (see **Figure 17(b)**). From the figure, it is seen that the contribution in attenuation which comes from contaminating by OH groups is unchanged after irradiation, while the one stemming from the presence of the Bi-dopants is substantially reduced.

One more example of the irradiation-induced bleaching effect is given in **Figure 18** where we make insight to the spectral transformations in the absorption peaks within the 750–950 nm band (“1”) after electron irradiation of the rest of Bi-doped germano-silicate fibers, Bi-1 and Bi-3. These two have, in pristine state, a higher and lower than Bi-2 concentration of BACs, correspondingly (see **Figure 17**). The spectra shown in **Figure 18** have been obtained before (dose “0”: black curves 1 and 3) and after (dose “3”: blue curves 2 and 4) electron irradiation. Qualitatively, the same law, viz., bleaching of the resonant-absorption peaks through the interval 750–950 nm as the result of electron irradiation, is revealed, now for fiber samples Bi-1 and Bi-3. Hence, the bleaching effect is found to be a general essence of the Bi-doped germano-silicate fibers.

The next graphs plotted in **Figure 19** (a, b) demonstrate how absorption peaks “1” (namely, its main subpeak centered at 820 nm) and “2” (the one centered at ~1400 nm) are reduced via electron irradiation (these dose dependences are shown for all fibers: Bi-1, Bi-2, and Bi-3). The initial absorption values (in peaks; these are given near each curve in **Figure 19(a, b)**) were taken from the attenuation spectra of pristine (dose “0”) samples. Curves 1–3 for resonant-absorption peaks “1” (**Figure 19(a)**) and “2” (**Figure 19(b)**) were obtained from the spectra shown in **Figures 16** and **17** after subtracting the background loss, which grows at irradiation (refer to **Figure 16** and also to **Figure 20**). Note that, for fiber Bi-3 characterized by the lowest content of Bi centers, the data are provided for peak “1” only because the measurements for peak “2” were below the resolution limit. It is seen from **Figure 19(a, b)** that bleaching of the resonant-absorption bands after electron irradiation is a characteristic feature of the Bi-doped germano-silicate fibers. Furthermore, resonant absorption bleaching in peaks “1” and “2” has almost the same character, which is evident from **Figure 19(c)** where we plot the ratio of absorption coefficients in peaks “1” and “2” in function of irradiation dose for Bi-1 and Bi-2 samples; see curve I. As seen, this quantity is kept virtually unchanged via irradiation, being equal to its initial value measured in pristine state. The same conclusion can be made for the ratio of absorption coefficients in peaks at ~500 nm and ~1400 nm (“2”), see curve II in **Figure 19(c)**. This is a justification of that resonant-absorption bands peaked at ~500, ~820, and ~1400 nm (and accordingly emission-active BACs attributed by these peaks, see **Figures 16–18**) are affected by the same or by a very similar manner by electron irradiation.

Then, as seen from **Figure 20**, the background loss (measured in the dip at 700 nm, between the absorption peaks ascribed to BACs in germano-silicate fiber; see **Figure 17**) monotonously increases with dose, a common effect for all kinds of Ge-doped silica materials. (Growth of the background loss is even more pronounceable in the UV.)

The results of electron irradiation of the Bi-doped alumino-silicate fibers (exemplified for fiber Bi-4) deserve a separate attention. **Figure 21** shows how the attenuation spectra of this fiber

are changed after a maximal dose of electron irradiation. It is seen from a direct comparison of curves 1 and 2 (obtained before and after irradiation) that in the Bi-doped aluminate fiber an opposite (to the case of the Bi doped germanate fiber) trend exists, viz. instead of resonant-absorption bleaching (see **Figures 17–19**), weaker but detectable extra absorption arises in the peaks centered at ~520 and ~700 nm. Inset to **Figure 21** examples the dynamics of the absorption peak at ~700 nm upon dose; note that almost the same dose behavior is observed for the peaks at ~520 and ~1050 nm.

We do not present here the results of measuring fluorescence spectra and fluorescence lifetimes adherent to BACs, obtained before and after irradiation; the reader is advised to refer to [67] for details. The only thing to mention in this regard is that the fluorescence spectra of both types of the Bi-doped fibers (germano- and alumino-silicate) were not affected qualitatively by electron irradiation, with a sole result of the latter being a decrease/increase of integrated fluorescence power emitted by the germano-/alumino-silicate fibers. Also note that almost no change was detected in the fluorescence kinetics for pristine and irradiated fibers of these two types ($0.38 \pm 0.03/0.89 \pm 0.04$ ms). Thus, the changes in the resonant-absorption peaks, detected above, should be related to a decrement/increment of the BACs concentration in the germanate/aluminate Bi-doped fibers.

4.3. Discussion

First of all, the attenuation spectra of typical pristine Bi-doped germano- and alumino-silicate fibers (**Figure 16**) need examination. From these spectra that cover an extended wavelengths interval (400–1600 nm), one can recognize the “fingerprints” of Bi dopants in the fibers, appearing through the correspondent resonant-absorption bands: these were referred to as Bi(Ge,Si) and Bi(Al) centers. Specifically, the main absorption peaks at 520, 700, and 1050 nm (the Bi-doped alumino-silicate fiber) seem to belong to the center Bi(Al), whereas the ones at 500, 820 (910), and 1400 nm (the Bi-doped germano-silicate fiber) — to physically similar Bi(Ge) and Bi(Si) BACs. Note that the peaks at 1400 nm look indistinguishable for both fiber types; so they can be related to Si forming host of both the glasses (see e.g. Refs. [68, 69]). (Other spectral features not linked to the presence in the fibers of Ge, Al, and Si originate either from contaminating by water (OH peaks at 1385 and 1240 nm) or from special design of the fibers (the cutoff peaks). Regarding the experimental results on electron irradiation, they are remarkable but not enough to make a definite conclusion on real processes involved. The only thing to propose is possible correlation of the rise and decrease of IR emission-active BACs concentrations after electron irradiation in alumino- and germano-silicate fibers, respectively, with known facts that substitutional four-coordinated Al in alumino-silicate glass is a hole trap, whereas substitutional Ge in germanate glass is an electron trap [64, 66, 70–72]. This difference can strongly affect the residuary charge state of the Bi specie after the electron irradiation. The process of radiation-induced charge trapping of both electrons and holes can be accompanied by the formation of different point defects (say, Ge(1), Ge(2), GeE', Al-E', and Al-ODCs [73, 74]), detectable in ESR and optical spectra' measurements.

5. Concluding remarks

Resuming, we have shown in this chapter that a diversity of effects can be encouraged at irradiating optical silica-based fibers with dopants of different kinds by high-energy β -electrons. This has been demonstrated on the examples of Ce- and Ce(Au)-doped alumino-phospho-silicate fibers, Yb-doped germano-alumino-silicate fibers, and Bi-doped germano- and alumino-silicate fibers. The data presented in this Chapter is a collection of our recent results, published in and in part reproduced from Refs [67, 75, 76]. In each case, unavoidable “darkening” of the fibers in VIS arises as the main feature of electron-irradiation. Meanwhile, such treatment allows one to detect interesting laws in transformations that “active” dopants presented in the fibers suffer as well as to propose mechanisms responsible for the phenomena involved. Also note that the new knowledge arising as the result of considering these transformations can be helpful for some applications of these or other doped fibers in such areas as dosimetry (on nuclear plants) and space technology and can be as well valuable when designing fiber devices (lasers and amplifiers) for the next-day telecom systems.

Acknowledgements

The author sincerely acknowledges the following people, contributing in the researches highlighted above: Dr. N.S. Kozlova (National University of Science and Technology (MISIS), Moscow, Russia)—for assistance in electron irradiation of all fibers; Drs. M.C. Paul and S. Ghosh (Central Glass & Ceramic Research Institute, Kolkata, India)—for providing samples of Ce and Ce(Au)-doped fibers and for discussions; Drs. V.V. Dvoyrin, V.M. Mashinsky, and E.M. Dianov (Fiber Optics Research Center of the Russian Academy of Sciences, Moscow, Russia)—for providing samples of Bi-doped fibers and valuable discussions; Dr. Yu.O. Barmenkov (Centro de Investigaciones en Optica, Leon, Mexico)—for participating in experiments with Ce and Ce(Au)-doped fibers and useful discussions. The author also thanks support from the Ministry of Education and Science of the Russian Federation under the “Increase Competitiveness Program of NUST «MISiS»” (Grant K3-2015-056).

Author details

Alexander V. Kir'yanov

Address all correspondence to: kiryanov@cio.mx

Centro de Investigaciones en Optica (Center for Optical Researches), Leon, Guanajuato, Mexico

References

- [1] Berthold III JW. Overview of prototype fiber optic sensors for future application in nuclear environments. *Proc. SPIE*. 1994; 2425: 74–83.
- [2] Berghmans F, Deparis O, Coenen S, Decréton M, Jucker P. Optical fibres in nuclear radiation environments: potential applications radiation effects need for standards. Soares ODD, editor. *Trends in Optical Fibre Metrology and Standards ...* (NATO ASI Series E: Applied Sciences). Springer (Netherlands); 1995; 285: 131–156. DOI: 10.1007/978-94-011-0035-9
- [3] Partin JK. Radiation response of optical fibers in a nuclear reactor. *Proc. SPIE*. 1984; 506: 46–49.
- [4] Liu P, Bao X, Brown K, Kulkarni N. Gamma-induced attenuation in normal single- and multi-mode, Ge-doped and P-doped optical fibers: A fiber optic dosimeter for low dose levels. *Can. J. Phys.* 2000; 78: 89–97.
- [5] Paul MC, Bohra D, Dhar A, Sen R, Bhatnagar PK, Dasgupta K. Radiation response behavior of high phosphorous doped step-index multimode optical fibers under low dose gamma irradiation. *J. Non-Crystal. Sol.* 2009; 355: 1496–1507.
- [6] Ghosh S, Das S, Paul MC, Dasgupta K, Bohra D, Chaudhary HS, Panwar L, Bhatnagar PK, Vijapurkar SG. Evaluation of the performance of high phosphorous with germanium codoped multimode optical fiber for use as a radiation sensor at low dose rates. *Appl. Opt.* 2011; 50: E80-E85.
- [7] Jones SC, Sweet JA, Braunlich P, Hoffman JM, Hegland JE. A remote fibre optic laser TLD system. *Rad. Prot. Dos.* 1993; 47: 525–528.
- [8] Houston AL, Justus BL, Falkenstein PL, Miller RW, Ning H, Altemus R. Remote optical fiber dosimetry. *Nuclear Instr. Meth. Phys. Res. B* 2011; 184: 55–67.
- [9] Canevali C, Mattoni M, Morazzoni F, Scotti R, Casu M, Musinu A, Krsmanovic R, Polizzi S, Speghini A, Bettinelli M. Stability of luminescent trivalent cerium in silica host glasses modified by Boron and Phosphorus. *J. Am. Chem. Soc.* 2005; 127: 42–50.
- [10] Nikl M, Nitsch K, Mihokova E, Solovieva N, Mares JA, Fabeni P, Pazzi GP, Martini M, Vedda A, Baccaro S. Efficient radioluminescence of the Ce³⁺-doped Na-Gd phosphate glasses. *Appl. Phys. Lett.* 2000; 77: 2159–2161.
- [11] Baccaro S, Dall'Igna R, Fabeni P, Martini M, Mares JA, Meinardi F, Nikl M, Nitsch K, Pazzi GP, Polato P, Susini C, Vedda A, Zanella G, Zannori R. Ce³⁺ or Tb³⁺ -doped phosphate and silicate scintillating glasses. *J. Lumin.* 2000; 87: 673–675.
- [12] Fu Q, Saltsburg H, Flytzani-Stephanopoulos M. Active-non-metallic Au and Pt species on Ceria-based water-gas shift catalysts. *Science*. 2003; 301: 935–938.

- [13] Wang X, Rodriguez JA, Hanson JC. In situ time-resolved characterization of Au-CeO₂ and AuO_x-CeO₂ catalysts during the water-gas shift reaction: Presence of Au and O vacancies in the active phase. *J. Chem. Phys.* 2005; 123: 221101.
- [14] Friebele EJ. Radiation protection of fiber optics materials: Effect of cerium doping on the radiation-induced absorption. *Appl. Phys. Lett.* 1975; 27: 210–212.
- [15] Anoikin EV, Guryanov AN, Gusovsky DD, Dianov EM, Mashinsky VM, Miroshnichenko SI, Neustruev VB, Tikhomirov VA, Zverev YB. UV and gamma radiation damage in silica glass and fibres doped with germanium and cerium. *Nuclear Instr. Meth. Phys. Res. B.* 1992; 65: 392–396.
- [16] Vedda A, Chiodini N, Di Martino D, Fasoli M, Keffer S, Lauria A, Martini M, Moretti F, Spinolo G, Nikl M, Solovieva N, Brambilla G. Ce³⁺-doped optical fibres for remote radiation dosimetry. *Appl. Phys. Lett.* 2004; 85: 6536–6538.
- [17] Chiodini N, Brambilla G, Vedda A, Di Martino D, Fasoli M, Lauria A, Redaelli M, Rosetta E. SiO₂ – based scintillating fibres for X-ray detection. *Proc. SPIE.* 2004; 5198: 298–305.
- [18] Cruz JL, Lliso-Valverde F, Andres MV, Perez-Calatayud J. Induced attenuation in Ce and Nd doped fibers irradiated with electron beams under low dose regime. *Opt. Commun.* 2005; 252: 286–291.
- [19] Mones E, Veronese I, Moretti F, Fasoli M, Loi G, Negri E, Brambilla M, Chiodini N, Vedda A. Feasibility study for the use of Ce³⁺-doped optical fibers in radiotherapy. *Nuclear Instr. Meth. Phys. Res. A.* 2006; 562: 449–455.
- [20] Mones E, Veronese I, Vedda A, Loi G, Fasoli M, Moretti F, Chiodini N, Canillo B, Brambilla M. Ce-doped optical fibre as radioluminescent dosimeter in radiotherapy. *Radiat. Measur.* 2008; 43: 888–892.
- [21] Broer MM, Cone RL, Simpson JR. Ultraviolet-induced distributed-feedback gratings in Ce³⁺-doped silica optical fibers. *Opt. Lett.* 1991; 16: 1391–1393.
- [22] Dong L, Archambault JL, Reekie L, Russel PSJ, Payne D. Bragg gratings in Ce³⁺-doped fibers written by a single excimer pulse. *Opt. Lett.* 1993; 18: 861–863.
- [23] Poignant H, Boj S, Delavaque E, Monerie M, Taunay T, Niay P, Bernage P, Xie WX. Ultraviolet-induced permanent Bragg gratings in Ce-doped fluorozirconate glasses or optical fibers. *J. Non-Crystal. Sol.* 1995; 184: 282–285.
- [24] Taunay T, Bernage P, Douay M, Xie WX, Martinelli G, Niay P, Bayon JF, Delavaque E, Poignant H. Ultraviolet-enhanced photosensitivity in cerium-doped aluminosilicate fibers and glasses through high-pressure hydrogen loading. *J. Opt. Soc. Am. B.* 1997; 14: 912–925.
- [25] Saad M, Chen LR, Gu X. Highly reflective fiber Bragg gratings inscribed in Ce/Tm co-doped ZBLAN fibers. *IEEE Photon. Technol. Lett.* 2013; 25: 1066–1068.

- [26] Farah K, Mejri A, Hosni F, Hamzaoui AH, Boizot B. Formation and decay of colour centres in a silicate glasses exposed to gamma radiation: Application to high-dose dosimetry. *Current Topics in Ionizing Radiation Research*, Nenoï M, editor. InTech (Croatia); 2012. DOI: 10.5772/32765
- [27] Engholm M, Jelger P, Laurell F, Norin L. Improved photodarkening resistivity in ytterbium-doped fiber lasers by cerium cooping. *Opt. Lett.* 2009; 34: 1285–1287.
- [28] Vivona M, Girard S, Marcandella C, Robin T, Cadier B, Cannas M, Boukenter A, Ouerdane Y. Influence of Ce codoping and H pre-loading on Er/Yb-doped fiber: radiation response characterized by Confocal Micro-Luminescence. *J. Non-Crystal. Solid* 2011; 357: 1963–1965.
- [29] Pask HM, Carman RJ, Hanna DC, Tropper AC, Mackechnie CJ, Barber PR, Dawes JM. Ytterbium-doped silica fiber lasers: versatile sources for the 1–1.2 μm region. *IEEE J. Quant. Electron.* 1995; 1: 2–13.
- [30] Richardson DJ, Nilsson J, Clarkson WA. High-power fiber lasers: current status and future perspectives. *J. Opt. Soc. Am. B.* 2010; 27: B63–B92.
- [31] Koponen JJ, Soderlund MJ, Hoffman HJ, Tammela SKT. Measuring photodarkening from single-mode ytterbium doped silica fibers. *Opt. Expr.* 2006; 14: 11539–11544.
- [32] Kirchhof J, Unger S, Schwuchow A, Grimm S, Reichel V. Materials for high-power fiber lasers. *J. Non-Crystal. Sol.* 2006; 352: 2399–2403.
- [33] Manek-Honninger I, Bouillet J, Cardinal T, Guillen F, Podgorski M, Bello Doua R, Salin F. Photodarkening and photobleaching of an ytterbium-doped silica double-clad LMA fiber. *Opt. Expr.* 2007; 15: 1606–1611.
- [34] Jetschke S, Unger S, Ropke U, Kirchhof J. Photodarkening in Yb doped fibers: experimental evidence of equilibrium states depending on the pump power. *Opt. Expr.* 2007; 15: 14838–14843.
- [35] Kitabayashi T, Ikeda M, Nakai M, Sakai T, Himeno K, Ohashi K. Population inversion factor dependence of photodarkening of Yb-doped fibers and its suppression by highly aluminum doping. In: *Optical Fiber Communications Conference; Anaheim, USA; 2006.* paper OThC5.
- [36] Guzman Chavez AD, Kir'yanov AV, Barmenkov YO, Il'ichev NN. Reversible photodarkening and resonant photo-bleaching of ytterbium-doped silica fiber at in-core 977 nm and 543 nm irradiation. *Laser Phys. Lett.* 2007; 4: 734–739.
- [37] Koponen J, Soderlund M, Hoffman HJ, Kliner DAV, Koplów JP, Hotoleanu M. Photodarkening rate in Yb-doped silica fibers. *Appl. Opt.* 2008; 47: 1247–1256.
- [38] Koponen J, Laurila M, Hotoleanu M. Inversion behavior in core- and cladding-pumped Yb-doped fiber photodarkening measurements. *Appl. Opt.* 2008; 47: 4522–4528.

- [39] Yoo S, Basu C, Boyland AJ, Sones C, Nilsson J, Sahu JK, Payne D. Photodarkening in Yb-doped aluminosilicate fibers induced by 488 nm irradiation. *Opt. Lett.* 2007; 32: 1626–1628.
- [40] Engholm M, Norin L, Aberg D. Improved photodarkening resistivity in ytterbium-doped fiber lasers by cerium cooping. *Opt. Lett.* 2009; 34: 1285–1287.
- [41] Engholm M, Jelger P, Laurell F, Norin L. Strong UV absorption and visible luminescence in ytterbium-doped aluminosilicate glass under UV excitation. *Opt. Lett.* 2007; 32: 3352–3354.
- [42] Suzuki S, McKay HA, Peng X, Fu L, Dong L. Highly ytterbium-doped silica fibers with low photo-darkening. *Opt. Expr.* 2009; 17: 9924–993.
- [43] Fox BP, Schneider ZV, Simmons-Potter K, Thomes Jr. WJ, Meister DC, Bambha RP, Kliner DAV, Soderlund MJ. Gamma radiation effects in Yb-doped optical fiber. *Proc. SPIE.* 2007; 6453: paper 645328.
- [44] Arai T, Ichii K, Tanigawa S, Fujimaki M. Gamma-irradiation-induced photodarkening in ytterbium-doped silica glasses. *Proc. SPIE.* 2011; 7914: paper 7914OK.
- [45] Groothoff N, Canning J, Aslund M, Jackson S. 193 nm photodarkening of ytterbium-doped optical fibre. In: *OSA/BGPP Meeting; 2007; paper BTuC2.*
- [46] Kir'yanov AV, Barmenkov YO, Lucio Martinez I, Kurkov AS, Dianov EM. Cooperative luminescence and absorption in ytterbium-doped silica fiber and the fiber nonlinear transmission coefficient at $\lambda=980$ nm with a regard to the ytterbium ion-pairs' effect. *Opt. Expr.* 2006; 14: 3981–3992.
- [47] Carlson CG, Keister KE, Dragic PD, Croteau A, Eden JG. Photoexcitation of Yb-doped aluminosilicate fibers at 250 nm: evidence for excitation transfer from oxygen deficiency centers to Yb³⁺. *J. Opt. Soc. Am. B.* 2010; 27: 2087–2094.
- [48] Burshtein Z, Kalisky Y, Levy SZ, Le Boulanger P, Rotman S. Impurity local phonon nonradiative quenching of Yb fluorescence in ytterbium-doped silicate glasses. *IEEE J. Quant. Electron.* 2000; 36: 1000–1007.
- [49] Peng M, Qiu J, Chen D, Meng X, Yang I, Jiang X, Zhu C. Bismuth- and aluminum-codoped germanium oxide glasses for super-broadband optical amplification. *Opt. Lett.* 2004; 29: 1998–2000.
- [50] Dianov EM, Dvoyrin VV, Mashinsky VM, Umnikov AA, Yashkov MV, Guryanov AN. CW bismuth fibre laser. *Quantum Electron.* 2005; 35: 1083–1084.
- [51] Peng M, Qiu J, Chen D, Meng X, Zhu C. Superbroadband 1310 nm emission from bismuth and tantalum codoped germanium oxide glasses. *Opt. Lett.* 2005; 30: 2433–2435.
- [52] Dvoyrin VV, Mashinsky VM, Bulatov LI, Bufetov IA, Shubin AV, Melkumov MA, Kustov EF, Dianov EM, Umnikov AA, Khopin VF, Yashkov MV, and Guryanov AN.

- Bismuth-doped-glass optical fibers – a new active medium for lasers and amplifiers. *Opt. Lett.* 2006; 31: 2966–2968.
- [53] Dianov EM, Shubin AV, Mel'kumov MA, Medvedkov OI, Bufetov IA. High-power CW bismuth fiber lasers. *J. Opt. Soc. Am. B.* 2007; 24: 1749–1755.
- [54] Rulkov AB, Ferin AA, Popov SV, Taylor JR, Razdobreev I, Bigot L, Bouwmans G. Narrow-line, 1178 nm CW bismuth-doped fiber laser with 6.4 W output for direct frequency doubling. *Opt. Expr.* 2007; 15: 5473–5476.
- [55] Razdobreev I, Bigot L, Pureur V, Favre A, Bouwmans G, Douay M. Efficient all-fiber bismuth-doped laser. *Appl. Phys. Lett.* 2007; 90: 031103.
- [56] Bufetov IA, Dianov EM. Bi-doped fiber lasers. *Laser Phys. Lett.* 2009; 7: 487–504.
- [57] Fujimoto Y, Nakatsuka M. Infrared luminescence from bismuth-doped silica glass. *Jpn. J. Appl. Phys.* 2001; 40: L279–L281.
- [58] Meng XG, Qiu JR, Peng MY, Chen DP, Zhao QZ, Jiang XW, Zhu CS. Near infrared broadband emission of bismuth-doped aluminophosphate glass. *Opt. Expr.* 2005; 13: 1628–1634.
- [59] Dvoyrin VV, Kir'yanov AV, Mashinsky VM, Medvedkov OI, Umnikov AA, Guryanov AN, Dianov EM. Absorption, gain, and laser action in bismuth-doped aluminosilicate optical fibers. *IEEE J. Quant. Electron.* 2010; 46: 182–190.
- [60] Peng M, Zhao Q, Qiu J, Wondraczek L. Generation of emission centers for broadband NIR luminescence in bismuthate glass by femtosecond laser irradiation. *J. Am. Ceram. Soc.* 2009; 92: 542–544.
- [61] Ou Y, Baccaro S, Zhang Y, Yang Y, Chen G. Effect of gamma-ray irradiation on the optical properties of $\text{PbO-B}_2\text{O}_3\text{-SiO}_2$ and $\text{Bi}_2\text{O}_3\text{-B}_2\text{O}_3\text{-SiO}_2$ glasses. *J. Am. Ceram. Soc.* 2010; 93: 338–341.
- [62] Griscom DL, Gingerich ME, Friebele EJ. Radiation-induced defects in glasses: Origin of power-law dependence of concentration on dose. *Phys. Rev. Lett.* 1993; 71: 1019–1022.
- [63] Médjahdi K, Boukenter A, Ouerdane Y, Messina F, Cannas M. Ultraviolet-induced paramagnetic centers and absorption changes in singlemode Ge-doped optical fibers. *Opt. Expr.* 2006; 14: 5885–5894.
- [64] Alessi A, Agnello S, Gelardi FM, Grandi S, Magistris A, Boscaino R. Twofold coordinated Ge defects induced by gamma-ray irradiation in Ge-doped SiO_2 . *Opt. Expr.* 2008; 16: 4895–4900.
- [65] Girard S, Ouerdane Y, Origlio G, Marcandella C, Boukenter A, Richard N, Baggio J, Paillet P, Cannas M, Bisutti J, Meunier JP, Boscaino R. Radiation effects on silica-based preforms and optical fibers—I: Experimental study with canonical samples. *IEEE Trans. Nucl. Sci.* 2008; 55: 3473–3482.

- [66] Dianov EM, Mashinsky VM, Neustruev VB, Sazhin OD, Brazhkin VV, Sidorov VA. Optical absorption and luminescence of germanium oxygen-deficient centers in densified germanosilicate glass. *Opt. Lett.* 1997; 22: 1089–1091.
- [67] Kir'yanov AV, Dvoyrin VV, Mashinsky VM, Il'ichev NN, Kozlova NS, Dianov EM. Influence of electron irradiation on optical properties of bismuth doped silica fibers. *Opt. Expr.* 2011; 19: 6599-6608.
- [68] Razdobreev I, El Hamzaoui H, Ivanov VY, Kustov EF, Capoen B, Bouazaoui M. Optical spectroscopy of bismuth-doped pure silica fiber preform. *Opt. Lett.* 2010; 35: 1341–1343.
- [69] Bufetov IA, Semenov SL, Vel'miskin VV, Firstov SV, Bufetova GA, Dianov EM. Optical properties of active bismuth centres in silica fibres containing no other dopants. *Quantum Electron.* 2010; 40: 639–641.
- [70] Skuja LN, Trukhin AN, Plaudis AE. Luminescence in germanium-doped glassy SiO₂. *Phys. Status Solidi A.* 1984; 84: K153–K157.
- [71] Griscom DL. Self-trapped holes in pure-silica glass: A history of their discovery and characterization and an example of their critical significance to industry. *J. Non-Cryst. Sol.* 2006; 352: 2601–2617.
- [72] Watanabe Y, Kawazoe H, Shibuya K, Muta K. Structure and mechanism of formation of drawing- or radiation-induced defects in SiO₂:GeO₂ optical fiber. *Jpn. J. Appl. Phys.* 1986; 25: 425–431.
- [73] Friebele EJ, Griscom DL, Sigel, Jr. GH. Defect centers in a germanium-doped silica-core optical fiber. *J. Appl. Phys.* 1974; 45: 3424–3428.
- [74] Trukhin AN, Sharakovski A, Grube J, Griscom DL. Sub-band-gap-excited luminescence of localized states in SiO₂-Si and SiO₂-Al glasses. *J. Non-Cryst. Sol.* 2010; 356: 982–986.
- [75] Kir'yanov AV, Ghosh S, Paul MC, Barmenkov YO, Aboites V, Kozlova NS. Ce-doped and Ce/Au-codoped alumino-phospho-silicate fibers: Spectral attenuation trends at high-energy electron irradiation and posterior low-power optical bleaching. *Opt. Mater. Expr.* 2014; 4: 434–448.
- [76] Kir'yanov AV. Electron-irradiation and photo-excitation darkening and bleaching of Yb doped silica fibers: comparison. *Opt. Photon. J.* 2011; 1: 155–166.